

Review Draft

An Evaluation of Hospital Radiation Detectors for Use in Screening Potentially Contaminated Individuals

Prepared by

R. Anigstein, M. C. Erdman, S. H. King, J. J. Mauro, and K. L. Miller

S. Cohen & Associates
6858 Old Dominion Drive
McLean, Virginia 22101

Under

Contract Number 200-2002-00367
Task Order Number 0003

Prepared for

Centers for Disease Control and Prevention
2920 Brandywine Rd.
Atlanta, GA 30341

Phillip Green
Project Officer

March 2005

Contents

	Page
1 An Evaluation of Hospital Radiation Detectors for Use in Screening Potentially Contaminated Individuals	1-1
1.1 Introduction	1-1
1.2 Materials and Equipment	1-1
1.2.1 Tissue-Equivalent Phantoms	1-1
1.2.2 Radioactive Sources	1-3
1.2.3 Gamma Cameras	1-4
1.2.4 Thyroid Uptake System	1-11
1.2.5 Portal Monitor	1-12
1.3 Radiation Measurements	1-14
1.3.1 Gamma Cameras	1-14
1.3.2 Thyroid Uptake System	1-22
1.3.3 Portal Monitor	1-24
1.4 Detector Response to Discrete and Distributed ¹³¹ I Source in Water-Filled Phantom	1-26
1.4.1 Gamma Cameras	1-26
1.4.2 Thyroid Uptake System	1-28
1.4.3 Portal monitor	1-29
1.5 Minimum Detectable Activity (MDA)	1-29
1.5.1 Phantom Studies	1-31
1.6 Calibration Factors	1-33
1.6.1 Gamma Camera	1-34
1.6.2 Thyroid Uptake System	1-35
1.6.3 Portal Monitor	1-36
1.6.4 Application of Results	1-36
1.7 Dose Calculations	1-36
1.8 Conclusions	1-38
References	1-38

Tables

1-1. Radioactive Sources Used in Study	1-5
1-2. Some Preset Radionuclide Energy Windows in the AXIS Camera System	1-10
1-3. AXIS Camera Parameters Used for Radionuclides in Present Study	1-11
1-4. Normalized Count Rates for Philips AXIS Camera and MDAs Using Various Counting Times for Sources in Acrylic Phantom	1-32
1-5. MDAs for Atomlab 950 Thyroid Uptake System Using Various Counting Times for Sources in Acrylic Phantom	1-33
1-6. MDAs for Portal Monitor System for Sources in Acrylic Phantom	1-34
1-7. Recommended Calibration Factors	1-36
1-8. Doses Associated with MDAs	1-37

Figures

	Page
1-1. Examples of Tissue-Equivalent Phantoms Used in Radiation Measurements	1-2
1-2. Acrylic Phantom: Schematic View of Components	1-2
1-3. View of Assembled Acrylic Phantom	1-3
1-4. Water-Filled Phantom	1-3
1-5. ¹³⁷ Cs and ⁶⁰ Co Sources (IPL 2003)	1-4
1- 6. ²⁴¹ Am Sources(NAS 2005)	1-4
1- 7. Source Holder for Ir-192	1-4
1-8. Philips AXIS Camera	1-6
1-9. Philips SKYLight Camera	1-6
1-10. Collimators in Rack	1-8
1-11. Back of Collimator Showing Corrugated Lead Strips	1-8
1-12. PHA screen on AXIS camera display console, showing a ⁶⁰ Co spectrum	1-9
1-13. Atomlab 950 Thyroid Uptake System	1-12
1-14. Atomlab 950 MCA Screen Showing Highlighted Region with ¹⁹² Ir Photopeaks	1-13
1-15. Schematic Diagram of Collimator on Atomlab Thyroid Uptake Probe	1-13
1-16. One Detector Assembly of the HMC Portal Monitor	1-14
1-17. AXIS Camera Showing Source Suspended from Meter Stick	1-15
1-18. AXIS Camera Showing Source Mounted in Acrylic Phantom	1-16
1-19. Normalized Count Rates in AXIS Camera from ¹³⁷ Cs in Air	1-17
1-20. Normalized Count Rates in AXIS Camera from ⁶⁰ Co Source in Air	1-18
1-21. Normalized Count Rates in AXIS Camera from ²⁴¹ Am Sources in Air	1-18
1-22. Normalized Count Rates in AXIS Camera from ¹⁹² Ir Source in Air	1-19
1-23. Normalized Count Rates in AXIS Camera from 1 µCi Sources in Acrylic Phantom . .	1-20
1-24. Normalized Count Rates in AXIS Camera with LEGAP collimator from 1 µCi Sources in Acrylic Phantom	1-21
1-25. Normalized Count Rates in AXIS Camera from 18 µCi ¹⁹² Ir Source in Phantom	1-21
1-26. Normalized Count Rates in Atomlab 950 Thyroid Uptake System from 1 µCi Sources in Air	1-22
1-27. Normalized Count Rates in Atomlab 950 Thyroid Uptake System from 18 µCi ¹⁹² Ir Source	1-23
1-28. Normalized Count Rates in Atomlab 950 Thyroid Uptake System from 1 µCi Sources in Acrylic Phantom	1-24
1-29. Normalized Exposure Rates Registered by Portal Monitor from Sources in Air	1-25
1-30. Normalized Count Rates, Converted from Portal Monitor Readings, from Sources in Acrylic Phantom	1-26
1-31. Count Rates in Philips Gamma Cameras from Discrete and Distributed ¹³¹ I Sources .	1-27
1-32. Count Rates in Atomlab 950 Thyroid Uptake System from Discrete and Distributed ¹³¹ I Sources	1-28
1-33. Exposure Rates on Portal Monitor from Discrete and Distributed ¹³¹ I Sources	1-30

Chapter 1

AN EVALUATION OF HOSPITAL RADIATION DETECTORS FOR USE IN SCREENING POTENTIALLY CONTAMINATED INDIVIDUALS

1.1 Introduction

The detonation of an improvised nuclear device or a radioactive dispersal device (RDD) would lead to wide-spread radioactive contamination, including the potential contamination of individuals. If such an event were to happen, it would be desirable to have various means of rapidly scanning individuals to determine if they have either external or internal contamination and to be able to determine when decontamination procedures have been successful. Nearly all hospitals provide nuclear medicine services for their patients. Therefore, most hospitals already possess various pieces of radiation detection equipment, including gamma cameras, thyroid uptake counters, Geiger-Mueller counters, and other portable radiation detection and measurement instruments. In addition, because of concerns over radioactivity inadvertently leaving the hospital in normal trash or over receiving patients in the emergency department who might be unknowingly contaminated with radioactive materials, a number of hospital have installed portal monitors that are capable of detecting low levels of radioactivity.

SC&A, Inc., in collaboration with the Hershey Medical Center (HMC), performed studies to evaluate radiation detection and imaging systems commonly found in hospitals, to determine their suitability for rapidly scanning individuals for internal contamination, and to develop recommendations regarding their potential use. The present report describes an evaluation of the potential use of nuclear medicine gamma camera systems, thyroid uptake counters, and portal monitors for detecting and measuring low levels of internal contamination. Later chapters will include specific recommendations and procedures for the use of this equipment in evaluating individuals potentially exposed to the inhalation of finely dispersed radioactive materials, and mathematical simulations of the response of gamma cameras to activity distributed in the lungs of an anthropomorphic phantom based on Reference Man.

1.2 Materials and Equipment

1.2.1 Tissue-Equivalent Phantoms

Phantoms for Use with Discrete Radioactive Sources

Various phantoms were potentially available for this study, including a tissue-equivalent Rando Phantom,¹ and a chest and torso phantom² used in the nuclear power industry for whole body counting (see [Figure 1-1](#)). However, these phantoms could not readily be loaded with the sources used for these measurements without permanently altering the phantom, such as by drilling larger holes, which made them unsuitable for use in the present study. To obviate these

¹ The Phantom Laboratory, P.O. Box 511, Salem, New York 12865-0511.

² Phantom courtesy of the Health Physics staff at the Three Mile Island Nuclear Power Station, Middletown, PA.

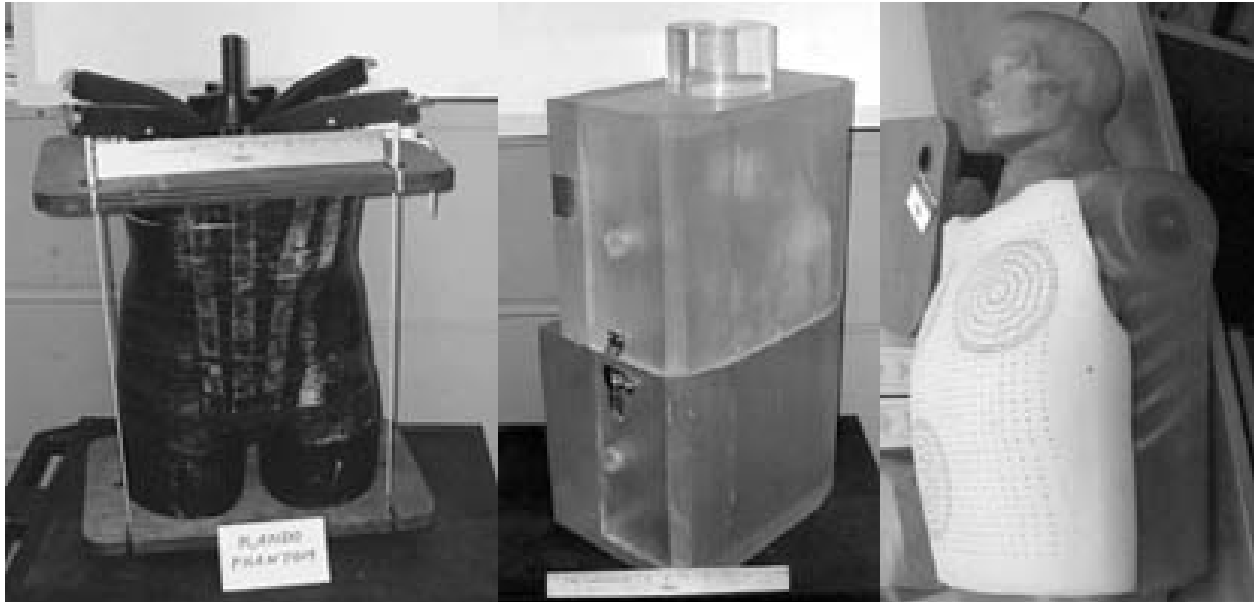


Figure 1-1. Examples of Tissue-Equivalent Phantoms Used in Radiation Measurements

difficulties, a simplified phantom was constructed from slabs of poly(methyl methacrylate) (PMMA), a clear plastic commonly known as acrylic and sold under various brand names, including Plexiglas®, Lucite®, and Acrylite®. PMMA has the empirical chemical formula $(C_5O_2H_8)_n$ and a typical density of 1.19 g/cm^3 .

Prior to adopting the acrylic phantom, its radiation absorption properties were compared to equal thicknesses of the Rando Phantom. When the results showed that equal thicknesses provided the same attenuation, the acrylic phantom was chosen for use in the present study. The phantom consists of a series of identical slabs, each 11.75×11.75 inches ($29.85 \times 29.85 \text{ cm}$), with a nominal thickness of $\frac{15}{16}$ in (2.38 cm). Up to ten of these slabs were used to simulate varying

thicknesses of tissue between the radiation source and the detector. The source, embedded in an acrylic disc, was

mounted at the center of an 11th slab. This source slab was identical to the others except for a hole in the center that is 1.125 inches in diameter and 0.375 inch deep ($2.86 \times 0.95 \text{ cm}$). A schematic view of the components of the phantom is presented in Figure 1-2—a photograph of the assembled phantom, comprising all 11 slabs,

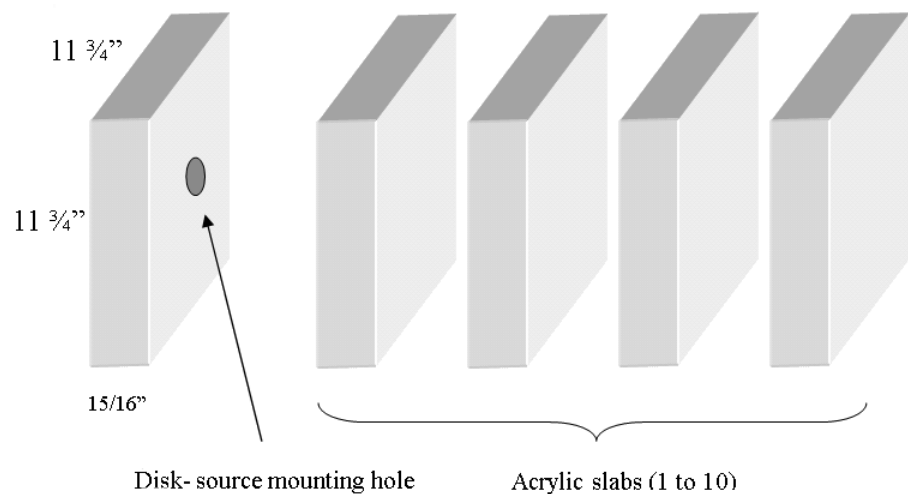


Figure 1-2. Acrylic Phantom: Schematic View of Components

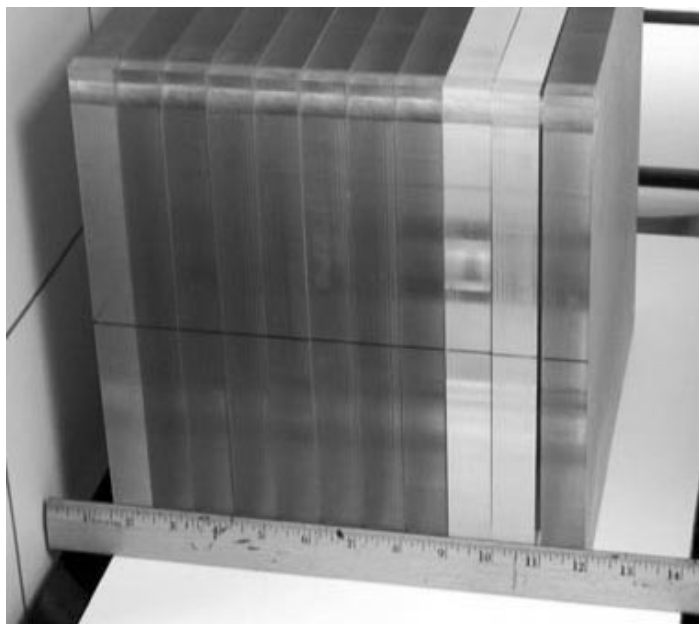


Figure 1-3. View of Assembled Acrylic Phantom



Figure 1-4. Water-Filled Phantom

is shown in [Figure 1-3](#). The hole for the disk source is visible in the photograph in the third slab from the right.

Phantom for Distributed Source

A water-filled container was used to compare the count rates from a discrete source, such as the ones used in the present study, and a source distributed over a volume which would correspond to a region of the human body. The container was a plastic jug, 28×16 cm by 38 cm high, filled with water to a depth of 34 cm (see [Figure 1-4](#)). ^{131}I was chosen for use in this comparison because it is readily available in aqueous solution and is commonly used in nuclear medicine. A discrete source was represented by an ampule containing ^{131}I that was placed in a plastic test tube filled with water and suspended in the water-filled jug by a wire at the center of the container. To measure the count rates from a distributed source, the ampule was broken and the jug thoroughly shaken, uniformly distributing the activity throughout the volume of water.

1.2.2 Radioactive Sources

The four radionuclides that were the principal focus of this study— ^{60}Co , ^{137}Cs , ^{192}Ir , and ^{241}Am —were selected from among those likely to be used in an RDD and which emit γ rays that span a wide range of energies. NIST-traceable sealed sources of ^{60}Co and ^{137}Cs were obtained from Isotope Products Laboratories, while NIST-traceable sources of ^{241}Am came from North American Scientific. Sources of each of these three radionuclides were procured with nominal activities of 1 or 10 μCi (37 or 370 kBq). Each of the ^{60}Co and ^{137}Cs sources consists of evaporated salts that were deposited at the bottom of a cylindrical cavity in an acrylic disk; the cavity was then plugged with an epoxy resin. The source itself comprises a thin disk, 5 mm in diameter, 2.77 mm from the face of the acrylic disk. The ^{241}Am source is in the form of a resin

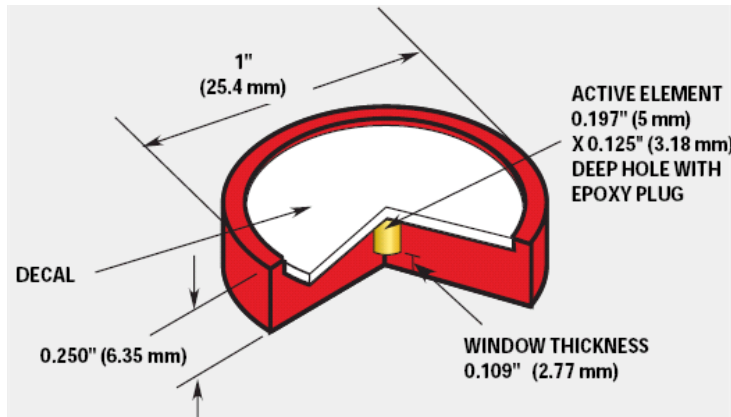


Figure 1-5. ^{137}Cs and ^{60}Co Sources (IPL 2003)

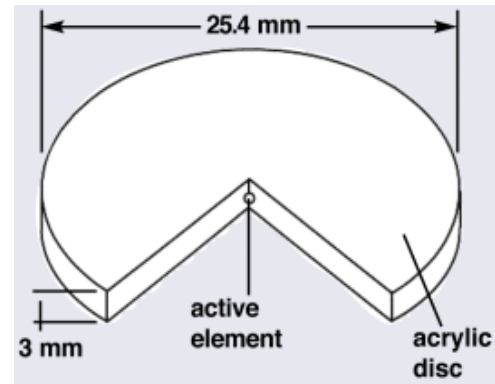


Figure 1- 6. ^{241}Am Sources (NAS 2005)

bead, 1 mm in diameter, mounted 1 mm from the surface of the disk. The source configurations are illustrated in Figures 1-5 and 1-6.

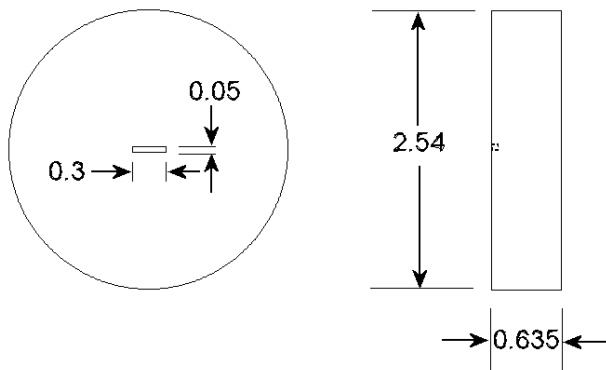


Figure 1- 7

Source Holder for Ir-192 (dimensions in cm)

^{192}Ir was not available as a NIST-traceable source. However, a relatively low-activity ^{192}Ir source was obtained in the form of a spent radiation therapy seed, with a strength of approximately 41 μCi , which decayed to about 18 μCi by the time of the experiments. The seed consisted of a 0.3-mm diameter core of 10% Ir–90% Pt, sealed inside a 0.1-mm-thick cylindrical platinum shell, 0.5 mm in outer diameter by 3 mm long. The shell was mounted lengthwise inside an acrylic disk to emulate as closely as possible the configuration of the NIST-traceable sources (see Figure 1-7).

In addition to the sealed sources, ^{131}I was obtained in aqueous solution, as discussed on page 1-3. This source had an initial activity of 16.7 μCi .

Detailed information on the sources and some of their radiological properties are presented in Table 1-1.

1.2.3 Gamma Cameras

The nuclear medicine gamma camera is also known as the Anger camera, after its inventor, Hal Anger. The camera consists of a collimator placed between the detector surface and the patient. The collimator is made primarily of lead and serves to suppress γ rays which deviate substantially from a direction perpendicular to the detector and thus acts as a type of "lens". The detector is a single crystal of NaI (sodium iodide), which produces light flashes of multiple photons when an impinging gamma ray interacts with the crystal. (Hence the name "scintillation camera" that is sometimes applied to this instrument.) The bursts of light flashes are detected by an array of photomultiplier tubes (PMTs) which are optically coupled to the surface of the

crystal. The output signal from the photomultipliers is an electrical current which is proportional to the energy of the gamma ray. Depending on the position of the event, the phototubes are variably activated. Hence, the entire system response yields positional information which is relatively accurate. The positional information is recorded using an analogue output onto film or a digital image is stored in a computer coupled to the camera. Since the total amount of energy deposited by a single gamma ray—and thus the net current generated by all photomultiplier tubes—is relatively constant, a deviation of the net current below a preset threshold signifies that the detected ray was degraded by Compton scattering. Use of a discrimination circuitry (i.e., a pulse-height analyzer) therefore permits suppression of Compton-scattered photons (Amersham 2004).

Table 1-1. Radioactive Sources Used in Study

Nuclide		Co-60	I-131	Cs-137	Ir-192	Am-241
Source Characteristics						
Activity (μCi)		1.007	56.03	0.9561	40.8	1.065
		10.2		9.745		9.102
Assay date		11-1-2004	11-18-2004	11-1-2004	10-18-2004	1-1-2005
Supplier ^a		IPL	NAS	IPL	Alpha-Omega	NAS
NIST-traceable?		Y	Y	Y	N	Y
Active diameter (cm)		0.5	N/A	0.5	N/A	0.1
Window	Material	Acrylic	N/A	Acrylic	Pt	Acrylic
	Thickness (cm)	0.277	N/A	0.277	0.05	0.1
Diameter of holder (cm)		2.54	N/A	2.54	2.54	2.54
Thickness of holder (cm)		0.635	N/A	0.635	0.635	0.3
Radiological Properties						
Half-life		5.27 y	8.02 d	30.07 y	73.83 d	432.2 y
Principal	Energy (keV)	1173.4	1332.5	364.5	661.7	296.0 – 612.5
Y-rays	Intensity	1	1	0.817	0.851	2.129 ^b
						0.359

^a NAS: North American Scientific, 20200 Sunburst Street, Chatsworth, CA 91311, www.nasmedical.com
IPL: Isotope Products Laboratories, 24937 Avenue Tibbitts, Valencia, CA 91355, www.isotopeproducts.com
Alpha Omega Services, Inc., 9156 Rose Street, Bellflower, CA 90706, <http://www.alpha-omegaserv.com/>

^b Total intensity of all γ radiation in this energy range

The NaI crystals in gamma cameras currently on the market range in thickness from 3/8 inch (0.95 cm) to 1 inch (2.54 cm). The thickness of the crystal can affect the detection efficiency of the system. High energy photons, such as those characteristic of ¹³⁷Cs and ⁶⁰Co, are more efficiently captured and detected by the thicker crystals. However, most current nuclear medicine diagnostic procedures use radionuclides that emit lower energy photons—the most common radionuclide used in nuclear medicine is ^{99m}Tc, which has a principal γ-ray energy of 140.5 keV. The 3/8-inch crystal has adequate sensitivity in this energy range, and is the one most commonly found in current gamma cameras.

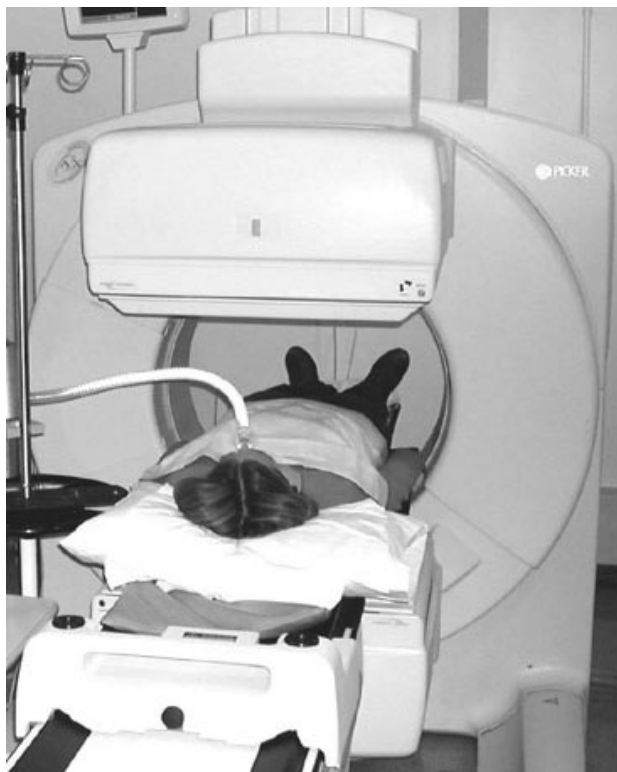


Figure 1-8. Philips AXIS Camera



Figure 1-9. Philips SKYLight Camera

Hershey Medical Center has six gamma cameras produced by Philips Medical Systems, N. A. These cameras comprise two models—the AXIS and the SKYLight—which are illustrated in [Figures 1-8 and 1-9](#). Four of the HMC cameras have $\frac{3}{8}$ -inch (0.95-cm) NaI crystals and two have $\frac{3}{4}$ -inch (1.9 cm) crystals. The AXIS camera, shown in Figure 1-8, has a field of view of 15.5×21 in (39.3×53.3 cm), while that of the SKYLight, shown in Figure 1-9, is 15×20 in (38.1×50.8 cm).³ Two different camera systems were used in the present study to provide a basis for comparing two different detector thicknesses: an AXIS system with a $\frac{3}{4}$ -inch crystal, and a SKYLight system with a $\frac{3}{8}$ -inch crystal. Most of the studies were performed on the AXIS system; the SKYLight studies were limited to the investigation of discrete and distributed sources in the water-filled phantom seen in [Figure 1-9](#).

Both the AXIS and SKYLight cameras have dual-head detector systems that allow the detector heads to be positioned at varying angles about the patient. The AXIS uses the conventional type of gantry on which the detector heads are mounted that allows the heads to be positioned at any angle about the patient, who typically lies on a table along the central axis of the detector gantry. The SKYLight system represents a newer design in which each detector head can be positioned independently of the other. Each camera system's computer performs acquisition, processing, display, archiving, and networking of the nuclear medicine data. The data in the present study

³ This is the field of view of the collimators, which are used for imaging in normal clinical practice. With the collimator removed, the field of view of the AXIS crystal is 16×21.5 in (40.7×54.7 cm).

represent count rates from one detector head at a time. In actual clinical practice, both detectors could be used to provide additional information.

Collimators

Collimators on gamma cameras and other radiation detectors used in nuclear medicine perform a function analogous to that of the glass lens in an optical camera. Radiation originating in discrete regions of the body is channeled to corresponding areas of the crystal. The scintillations (flashes of light) emitted in the crystal at the point a photon is absorbed or scattered from a short-lived image which is recorded by the photomultiplier tubes and the associated electronics and computer system. This image is used to create a map of the distribution of radionuclides in the region of interest—the organs or portions of the body that are the subject of the study.

Collimators on the AXIS system are made of a 95%-5% lead-antimony alloy. The collimator is a flat plate, about 1 inch (2.54 cm) thick, that is placed against the NaI crystal. It has a core that consists of a honeycomb of parallel holes.⁴ Photons that are normally incident on (i.e., perpendicular to) the plane of the collimator pass through the holes and are recorded as part of the image. Photons striking at an oblique angle are absorbed by the collimator or scattered away from the crystal. The design of the collimator is dictated by the γ -ray energies of the radionuclides used for the imaging study. Higher energies require thicker collimators, with thicker septa (the separations between the holes).

Several collimators are available for each type of camera system, including low energy (< 200 keV), medium energy (200 – 400 keV), high energy (400 – 600 keV), and pinhole collimators. The collimators used in most routine diagnostic studies are the low energy type, often referred to as the Low Energy All Purpose (LEAP) collimator (see [Figures 1-10 and 1-11](#)). The LEGAP collimator used with the AXIS camera is of this type, as is the LEGP collimator used with the SKYLight.

Collimators enable gamma cameras to image the distribution of radionuclides in the body, the main function of these instruments in nuclear medicine. However, in the contemplated use of these instruments to screen individuals who inadvertently inhaled airborne radioactive materials, collimators, which by design have a narrow angle of acceptance, would shield out most of the γ -ray photons and thus decrease the sensitivity of the detector system. Removal of the collimator improves the sensitivity of the camera; however, it also increases the background count rate. Since the minimal detectable activity (MDA) is a function of both the counting efficiency and the background count rate, we studied the response of the cameras both with and without collimators to determine the MDAs and thus the optimum use of the systems for the contemplated purpose.

⁴ Parallel holes produce an image that has the same size as the region of interest. Collimators with divergent-convergent holes can be used to enlarge or reduce the image.



Figure 1-10. Collimators in Rack



Figure 1-11. Back of Collimator Showing Corrugated Lead Strips

Pulse Height Analyzer

The typical radionuclide used in nuclear medicine emits a principal γ ray with a single energy that is used for imaging the distribution of that nuclide in a patient. When a γ ray interacts with the NaI crystal, the resulting scintillation is proportional to the energy of the incident photon. The electrical signal produced by the PMTs is in turn proportional to the scintillation. However, because of variations in the efficiency of converting the γ -ray energy to light photons, as well as in the efficiency of converting the light pulse to an electrical current, even monoenergetic γ -ray photons produce a spectrum of electrical pulses. The camera system incorporates a pulse height analyzer (PHA) that can be adjusted to allow only the range of pulses corresponding to a given γ -ray energy to be counted by the camera system and subsequently used to form the image.

In addition to the distribution of pulse heights corresponding to the direct interaction of the principal γ ray with the NaI crystal, the spectrum also includes events of lower energies. These include the escape peak—the energy deposited in the crystal when a K-shell x ray, with an average energy of 29 keV, emitted by the iodine atom escapes from the crystal. The energy of the escape peak is therefore 29 keV lower than the photopeak energy. More prominently, lower energy pulses are generated when γ -ray photons undergo Compton scattering in the patient's body outside the region of interest or by the collimator or other parts of the camera housing.

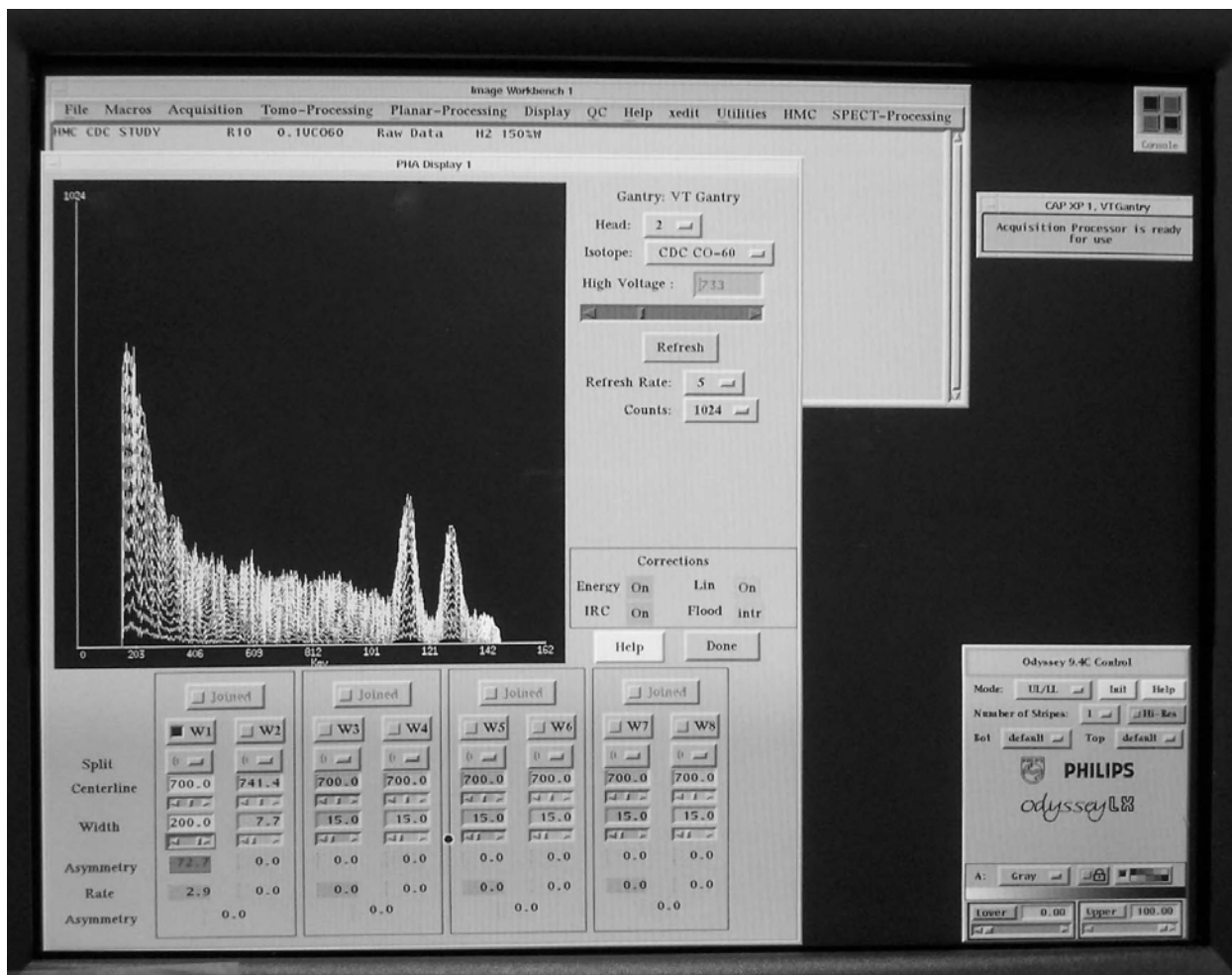


Figure 1-12. PHA screen on AXIS camera display console, showing ^{60}Co spectrum

Since these photons would contribute noise in the image being generated by the camera, the PHA is normally adjusted to reject the corresponding pulses.

Accessing the PHA on the AXIS camera's computer, as shown in [Figure 1-12](#), allows the user to view the pulse height spectrum and to adjust current energy setting. The scale is set to display the energies of the corresponding γ rays. The energy range is normally centered on the primary photopeak(s) of the radionuclide of interest. The width is typically set to equal 20% of the photopeak energy, meaning that pulses corresponding to energies $\pm 10\%$ of the true γ -ray energy are accepted by the PHA. The camera system includes factory-installed energy windows corresponding to radionuclides commonly used in nuclear medicine. Some of the preset energy windows found in the AXIS system are shown in [Table 1-2](#).

Radionuclide windows that are not preset can be programmed into the camera's computer. The nuclear medicine technologist has ready access to the predefined energy settings in the setup menu for each patient diagnostic acquisition. It is usually possible for him or her to alter the energy range for these preset radionuclide windows. It is *sometimes* possible for the technologist

to enter custom, i.e. user-defined, windows for radionuclides that do not appear on the factory-installed list, and save these as new radionuclide windows. For example, ^{137}Cs may be found as a predefined setting on some cameras, but not on others. On the AXIS camera, the procedure to add a new radionuclide is fairly straightforward. On the SKYLight camera system, adding a new radionuclide or modifying the energy range for an existing radionuclide requires password access to the Administrator section of the computer system. This section is rarely used by technologists or field engineers, so the password may not be commonly known. In either case, temporary adjustments to the centerline energy and the window width may be possible if the technologist is sufficiently familiar with the camera system.

In the AXIS camera system, the maximum peak energy—the energy that would normally correspond to the photopeak or the center of the photopeaks of the nuclide in question—that can be set in the PHA is 700 keV. However, higher-energy photons can be counted by setting the energy range to “200%.” This setting is a shorthand reference to the actual energy window. To understand this setting, we note that the PHA displays the histogrammed energy response of the activity seen by the detector. The scale can be expressed in channels (arbitrary binning units). For display purposes, the range is 0 – 256 on the horizontal axis. For a nuclide with a single γ ray, the centerline of the photopeak is set to Channel 110. Only pulses in Channels 25 – 231 are displayed and counted by the system. Thus, with the centerline of the “200%” window set to 700 keV, the maximum energy, which corresponds to Channel 231, is 1470 keV ($700 \times 231 \div 110 = 1470$), while the minimum energy for this setting is 159 keV. Thus, ^{60}Co , with principal γ -ray energies of 1173.4 and 1332.5 keV, falls within this energy window. The entire ^{60}Co spectrum, including the two principal photopeaks and the lower-energy Compton-scattered photons, is visible in the display in [Figure 1-12](#). The AXIS camera, if properly adjusted, can thus be used to detect and identify all the radionuclides in the present study.

Table 1-2. Some Preset Radionuclide Energy Windows in the AXIS Camera System

Nuclide	Peak Energy (keV)	Window (%)	Energy Range (keV)
F-18	511	20	409 – 613
Co-57	121.9 ^a	15	103.6 – 140.2
Tc-99m	140.5	15	119.4 – 161.6
I-131	364	20	291 – 437
Xe-133	81	20	64.8 – 97.2
Tl-201	75	40	45.0 – 105.0

Source: Marconi Medical Systems, Inc. 2001

^a Actual γ energy: 122.06 keV

The PHA of the SKYLight camera system can be set to encompass energies up to 920 keV. This enables the system to record the principal photopeaks for ^{131}I , ^{137}Cs , ^{192}Ir , and ^{241}Am . However, in the case of ^{60}Co , only Compton-scattered photons with energies < 920 keV can be counted.

Many of the radionuclides that are likely to be used in an RDD are not included in the list of factory-installed energy windows on gamma cameras. However, predefined energy windows can usually be adjusted to encompass the gamma spectrum for these radionuclides. Rather than define a new radionuclide as a custom addition, it may be easier to utilize radionuclides in the predefined list and simply expand the acquisition width to encompass the photopeaks of the nuclide of interest. [Table 1-3](#) lists the radionuclides included in the present study and the recommended settings for their detection.

Table 1-3. AXIS Camera Parameters Used for Radionuclides in Present Study

Actual Radionuclide	Principal γ -ray Energies (keV)	Preset Radionuclide	AXIS Energy Window	
			%	keV
Co-60	1173.4, 1332.5	Cs-137	20	595 – 728
			100	331 – 992
Cs-137	661.7	Cs-137	20	595 – 728
Ir-192	296.0 – 612.5	F-18	100	256 – 767
Am-241	59.5	Xe-133	100	40.5 – 121.5

1.2.4 Thyroid Uptake System

The Hershey Medical Center's Atomlab 950 Thyroid Uptake System, made by Biodex Medical Systems, Inc., is typical of the thyroid counting systems used in nuclear medicine departments. This system, shown in [Figure 1-13](#), consists of a 2×2 in (5×5 cm) NaI detector coupled to a 1024-channel multi-channel analyzer (MCA), shown in [Figure 1-14](#). The MCA, analogous to the PHA on the Philips gamma cameras, has factory-installed settings for approximately 23 radionuclides, and can accept 50 additional user-defined nuclides. The preprogrammed nuclides include ^{60}Co , ^{131}I , ^{137}Cs , and ^{192}Ir . For the purpose of the present study, ^{241}Am was added to the MCA radionuclide database, with a photopeak energy of 60 keV and an energy window with a range of 15 to 75 keV.

The NaI detector is typical of detectors on thyroid counting systems, and is shielded with a conventional flat-field lead collimator that meets IAEA specifications. The design of the collimator and the position of the NaI crystal are shown in the schematic diagram in [Figure 1-15](#). The inside diameter of the front edge of the collimator is approximately 3.6 in (9.1 cm), with a thickness of about 0.2 in (0.48 mm) on the outer rim. The cavity inside the collimator is in the shape of a 6-in-long (15.2 cm) truncated cone. The base of the cone is 3.625 in (9.2 cm) in diameter, while the opposite face has a diameter of 2 in (5.1 cm). The remaining dimensions are shown in the diagram. The collimator shields both the detector and the photomultiplier tube, minimizing the effects of background radiation. In [Figure 1-13](#), the probe is pointed in a horizontal direction for use with patients who are sitting upright. In the orientation shown in the [Figures 1-13](#) and [1-15](#), the detector is facing left.



Figure 1-13. Atomlab 950 Thyroid Uptake System

1.2.5 Portal Monitor

Hershey Medical Center uses a Ludlum Model 375-30 Waste Monitor as a portal monitor. This monitor, shown in [Figure 1-16](#), includes a pair of NaI crystals, 1 inch thick by 3 inches in diameter (2.54×7.62 cm), that face each other across a doorway. The detectors are shielded by a 0.71-in (1.8 cm) layer of lead. Each detector assembly is mounted on an independent frame that is mounted on wheels. The detectors share a single digital alarming rate meter (Ludlum Model 375 Digital Area Monitor). A Star DP8340 dot matrix printer is attached to the rate meter's serial output. In addition to the printer log, each alarm trip produces an audible alarm. At HMC, this system is located in a corridor through which all trash and laundry carts must pass on their way from the hospital portion of the facility to the processing area. The cabinet openings are fitted with acrylic panels to prevent unauthorized access to the electronics and the detector mounting bolts. The distance separating the two detectors is approximately 80 inches (2 m). Because of the protective panel, the closest allowable approach to either detector is 4.5 cm.

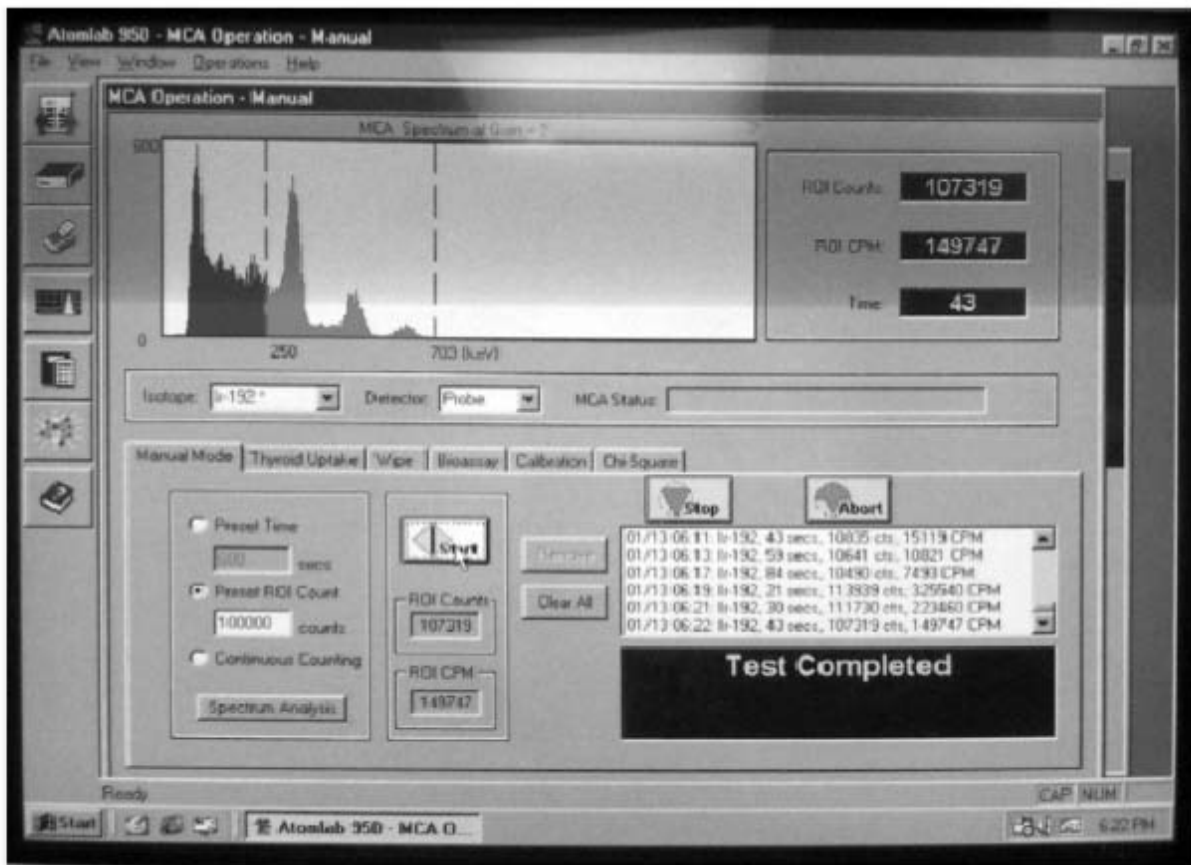


Figure 1-14. Atomlab 950 MCA Screen Showing Highlighted Region with ^{192}Ir Photopeaks

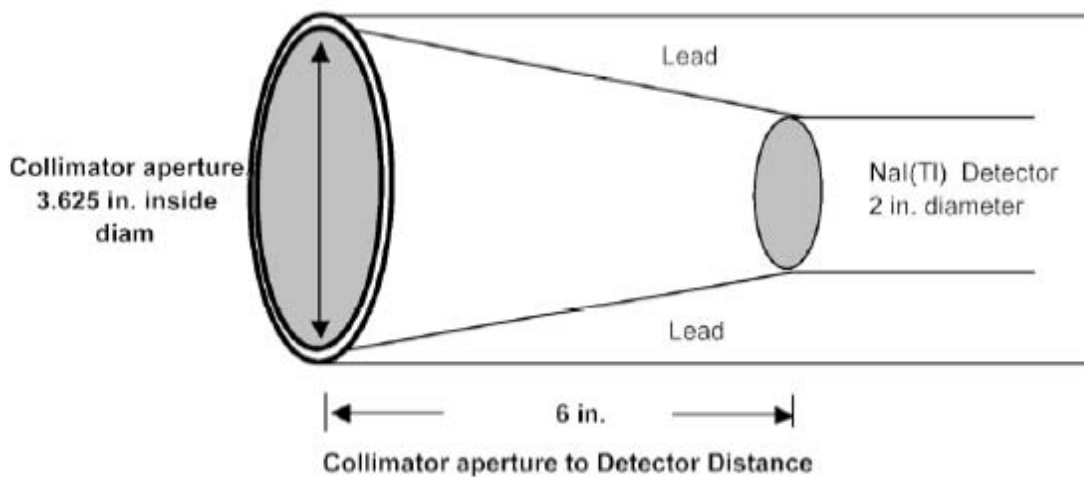


Figure 1-15. Schematic Diagram of Collimator on Atomlab Thyroid Uptake Probe



The system is located one floor below ground level. The background radiation at this location was measured to be 2.5 to 3.0 $\mu\text{R/hr}$ from both detectors combined, and approximately 1.5 $\mu\text{R/hr}$ with only one detector connected. An alarm setpoint of 10 $\mu\text{R/hr}$ is normally used with this system. This alarm set-point corresponds to 3 – 4 times background and was chosen to minimize alarms due to small variations or spikes in the noise level of the instrument. According to the manufacturer's specifications, the response time of the Model 375 ratemeter is typically 3 s from 10% to 90% of the final reading. When a $^{99\text{m}}\text{Tc}$ source was placed in the center of a loaded trash or laundry cart, shielding effects from the plastic trash and laundry carts used at this facility were found to be negligible. Through experimental measurements it was determined that the detector sensitivity for $^{99\text{m}}\text{Tc}$ at the center of a trash cart placed midway between the detectors, is approximately 11 μCi (407 kBq).

The simultaneous use of both detectors provides greater sensitivity and allows for patients to be directed through the doorway containing the detectors. To facilitate the analysis and interpretation of data collected in the present study, radiation measurements were performed with only one detector connected.

Figure 1-16. One Detector Assembly of the HMC Portal Monitor

1.3 Radiation Measurements

1.3.1 Gamma Cameras

Sources in Air

Count rates were recorded by the AXIS camera from sources in air at various distances from the detector. [Figure 1-17](#) shows the source, suspended from a meter stick, between the two heads of the AXIS camera. The collimator was removed from the head on the left. [Figure 1-18](#) shows the acrylic phantom in position between the detector heads—the head on the left has the collimator in place. The 1-inch button source is shown mounted in the outermost slab of the phantom.



Figure 1-17. AXIS Camera Showing Source Suspended from Meter Stick

^{137}Cs . Figure 1-19 shows the normalized count rates of the AXIS camera with a $\frac{3}{4}$ -inch crystal, with and without the LEGAP collimator, from a nominal $1\ \mu\text{Ci}$ ^{137}Cs source in air. The counts from the source, as well as background counts, were collected over a 2-minute interval, using the energy setting listed in [Table 1-3](#). The count rates, with the background subtracted, are normalized to a unit activity of the source, based on the decay-corrected source activity at the time of the experiment. The change in count rate as a function of distance from the detector is primarily a function of the solid angle subtended by the exposed area of the NaI crystal at the position of the source, and to a much smaller extent to the attenuation by the air between the source and the detector. With the collimator in place, the count rate is reduced by a factor of 5, due to the absorption and scattering of photons by the collimator. Any low-energy Compton-scattered photons that may have reached the NaI detector were rejected by the 20% energy window and were therefore not counted.



Figure 1-18. AXIS Camera Showing Source Mounted in Acrylic Phantom

^{60}Co . Count rates of the AXIS camera from a nominal $1\ \mu\text{Ci}$ ^{60}Co were recorded using methods similar to those used for the ^{137}Cs determinations. The study utilized the two energy windows listed in Table 1-3. One set of count rates used the window centered on the ^{137}Cs photopeak but with a 100% window.⁵ The experiment was repeated with a 20% window centered on the same photopeak, thus reproducing the conditions used in the ^{137}Cs source measurements. Since neither of the energy ranges encompassed the two principal ^{60}Co γ rays, the recorded counts were due entirely to the Compton-scattered photons that were generated when the primary photons interacted with various materials, primarily the lead shielding in the two detector heads. These results are shown in Figure 1-20. The narrower energy window reduced the count rates by a

⁵ Instructions for setting the “200%” window were obtained from Philips Medical Systems after this study was completed.

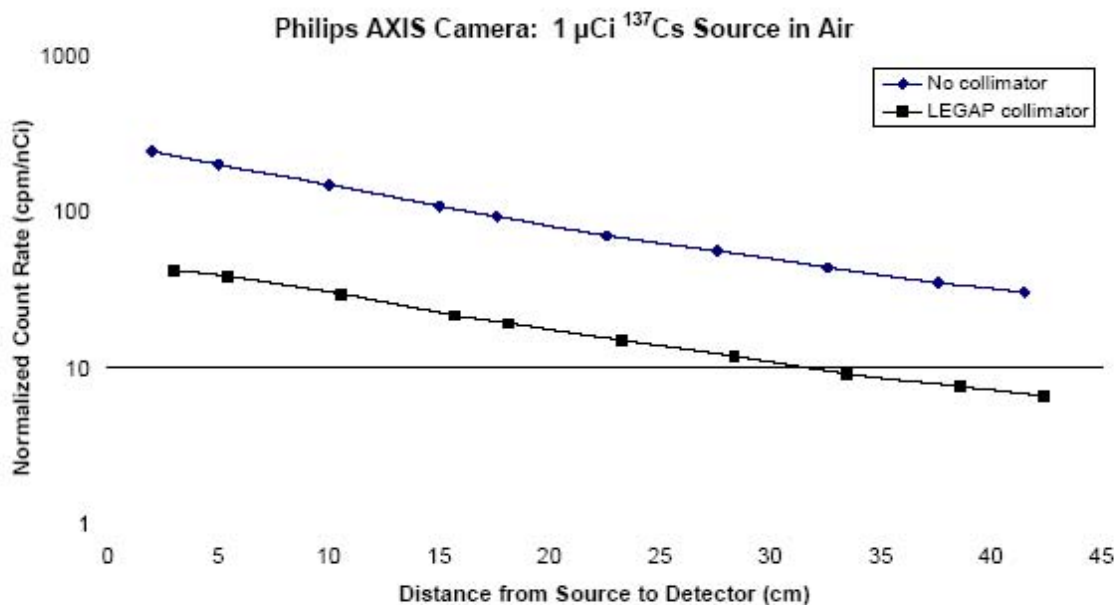


Figure 1-19. Normalized Count Rates in AXIS Camera from ^{137}Cs in Air

factor of 5, which suggests that the Compton spectra were more-or-less uniformly distributed over this energy range, since the 20% window has about 20% of the count rate registered with the 100% window. Unlike the case of the ^{137}Cs measurements, the collimator reduced the count rate by less than a factor of 2 in both energy windows. This is due partly to the greater penetrating power of the ^{60}Co γ rays, and also to the fact that the collimator contributes to the buildup of the Compton-scattered photons that are recorded in these windows.

^{241}Am . Count rates were recorded on the AXIS camera from ^{241}Am sources with nominal activities of 1 and 10 μCi . Figure 1-21 presents the normalized count rates, collected in a 100% ^{133}Xe window (see Table 1-3). This energy range was selected because ^{133}Xe is commonly used in nuclear medicine imaging procedures; consequently, the settings for this radionuclide are programmed into most gamma cameras, unlike those for ^{241}Am . The principal γ -ray energy of ^{133}Xe is 81 keV, which is about 36% higher than the 59.5 keV γ ray emitted by ^{241}Am . Expanding the width of the ^{133}Xe window to 100% results in an energy range of 40 to 122 keV, thus encompassing the ^{241}Am γ ray. While an ^{241}Am window could be designed and stored in the camera's computer, utilizing an existing radionuclide window and extending its width is a simpler process in a quick response environment. For the in-air measurements with no collimator, the drop off in the normalized count rate from the 10 μCi source close to the crystal, as seen in Figure 1-21, is most likely the result of dead time due to the excessively high counting rate. However, with the use of a LEGAP collimator, the count rate was not significantly different from the count rate of the background. The use of a collimator would therefore be inappropriate for assessing ^{241}Am activities.

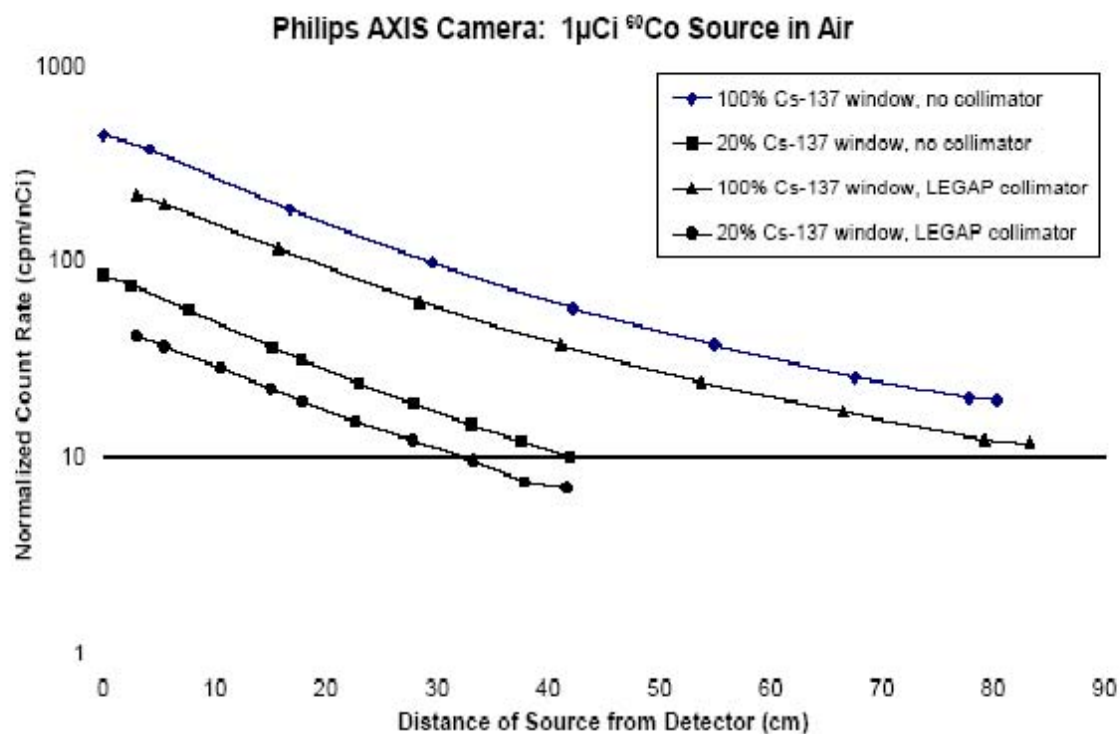


Figure 1-20. Normalized Count Rates in AXIS Camera from ^{60}Co Source in Air

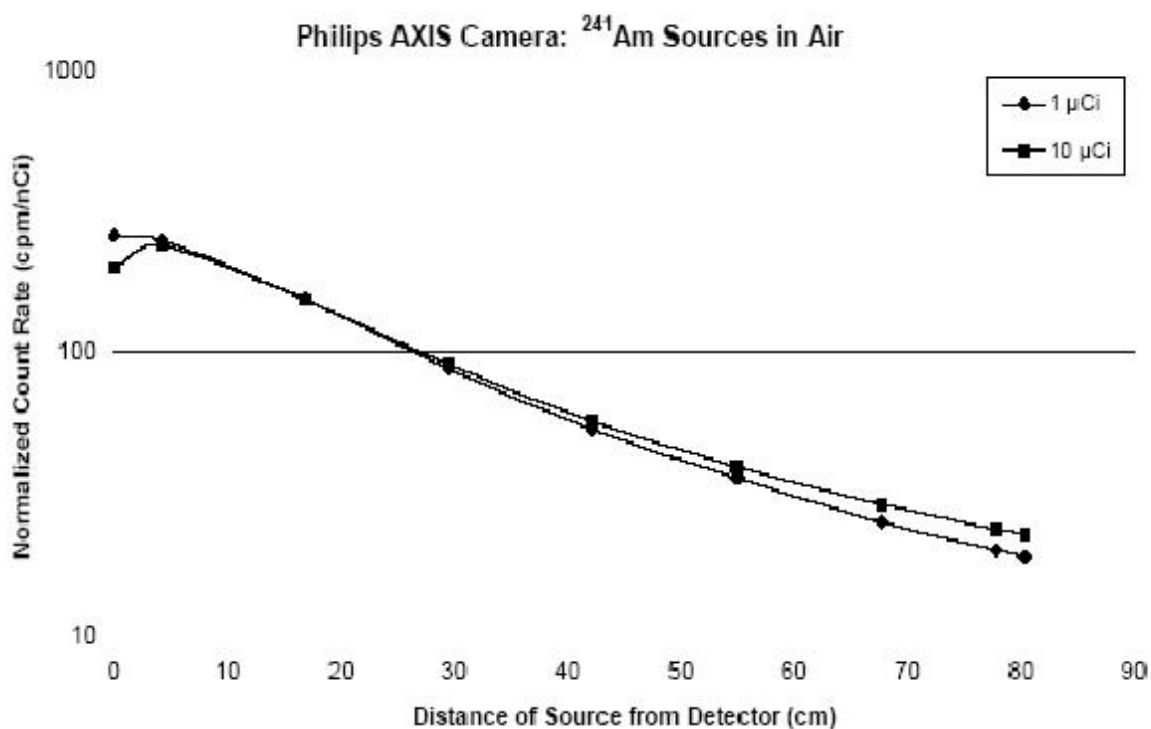


Figure 1-21. Normalized Count Rates in AXIS Camera from ^{241}Am Sources in Air

¹⁹²Ir. Figure 1-22 presents the normalized count rates in the AXIS system from a discrete source of ¹⁹²Ir with an activity of approximately 18 μ Ci at the time of the measurements, counted in a 100% ¹⁸F energy window, as listed in Table 1-3. As is the case for ²⁴¹Am, ¹⁹²Ir is not used for nuclear medicine imaging studies and is therefore not normally programmed into the gamma cameras. The ¹⁸F window, expanded to 100%, has an energy range of 255 to 766 keV. This range encompasses over 91% of the complex γ -ray spectrum of ¹⁹²Ir. The LEGAP collimator reduces the count rates by about an order of magnitude.

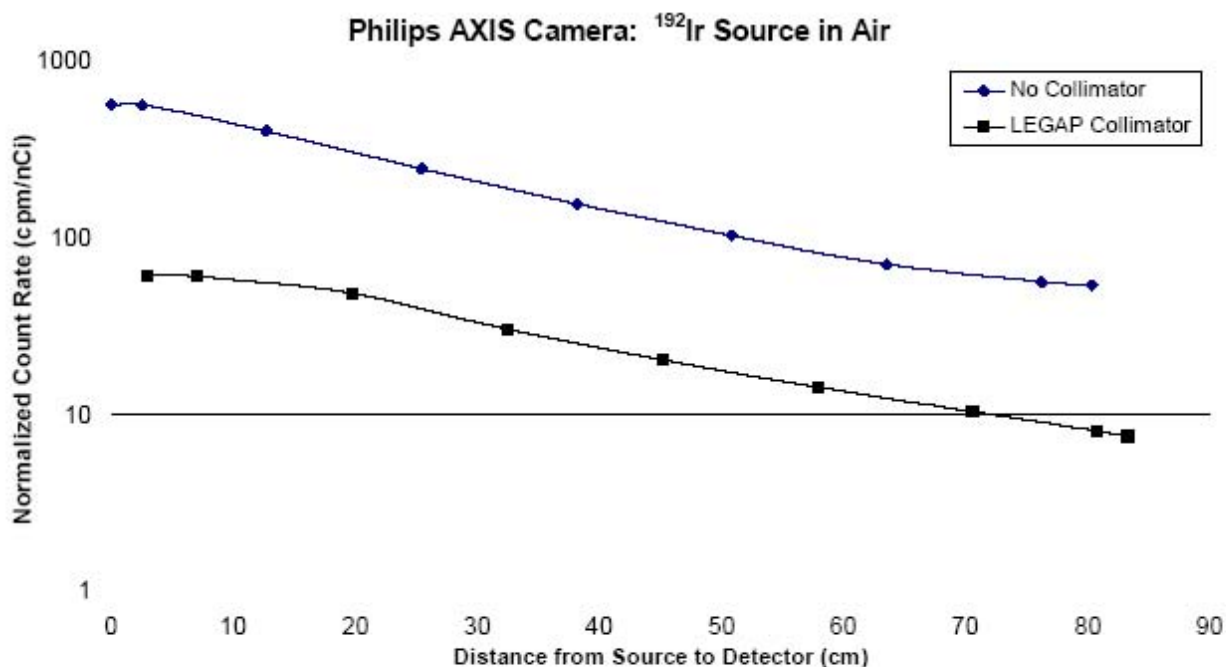


Figure 1-22. Normalized Count Rates in AXIS Camera from ¹⁹²Ir Source in Air

Sources in Acrylic Phantom

Count rates were recorded on the AXIS camera from sources at different depths within the acrylic phantom. In the first set of experiments, the phantom was placed with the front face 7.6 cm from the face of the detector window, with no collimator. ⁶⁰Co, ¹³⁷Cs, and ²⁴¹Am sources with nominal activities of 1 μ Ci were placed in successive positions within the phantom. The minimum absorber between the source and the detector was the aluminum window on the detector plus the thin acrylic window on the 1-inch disk source (see page 1-4) while the maximum included the total thickness of the acrylic phantom—about 26 cm. The same energy windows were used as in the in-air measurements, except that only the 100% ¹³⁷Cs window was used to record counts from the ⁶⁰Co source.

The resulting normalized count rates are presented in Figure 1-23. The first point on the left end of each curve represents the source with minimum attenuation. Each successive point corresponds to an additional 2.4-cm-thick slab of acrylic. The total thickness of the attenuating acrylic phantom can be determined from subtracting the 7.6-cm air gap between the phantom

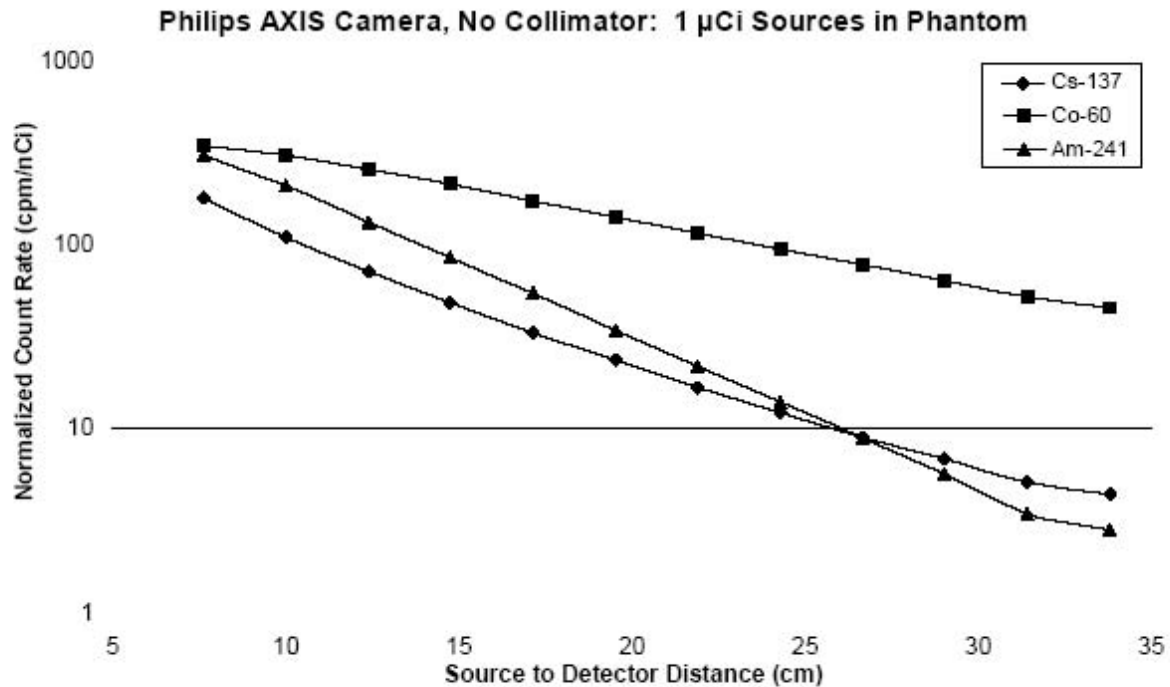


Figure 1-23. Normalized Count Rates in AXIS Camera from 1 μ Ci Sources in Acrylic Phantom

and the detector from the distance between the source and the detector that is listed on the X-axis.

Next, the collimator was replaced on the camera and the set of measurements was repeated. In this experiment, the front face of the phantom was placed 8.9 cm from the face of the collimator. Since the collimator assembly is approximately 2.7 cm thick, the phantom was 11.6 cm from the detector window. As was noted earlier, a 1- μ Ci source of ^{241}Am cannot be reliably detected with the LEGAP collimator in place; therefore, these measurements were performed only on ^{60}Co and ^{137}Cs . The same energy windows were used as in the measurements without a collimator. The results are shown in [Figure 1-24](#). The use of the collimator reduces the count rate from ^{60}Co by about a factor of 2. The ^{137}Cs count rate is reduced about 5-fold.

The phantom studies were repeated, using the 18 μ Ci ^{192}Ir source. The results are displayed in [Figure 1-25](#). The collimator produces a 6-to-8-fold reduction in the count rate.

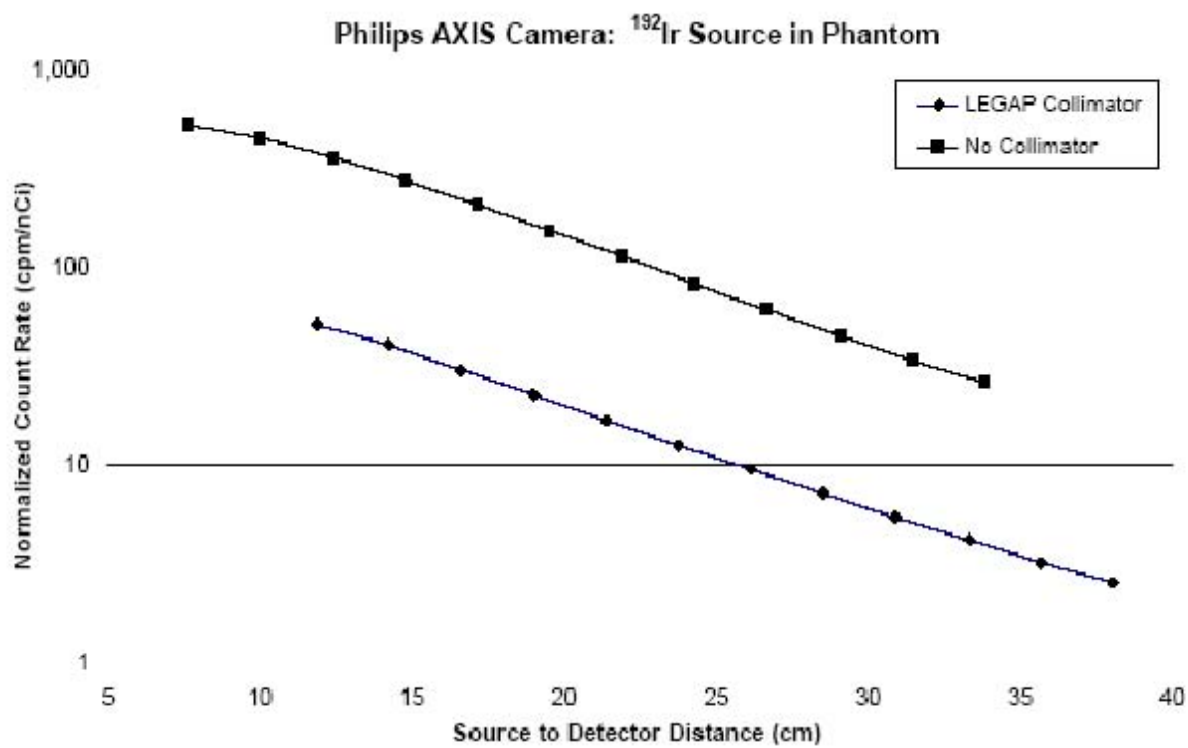


Figure 1-24. Normalized Count Rates in AXIS Camera with LEGAP collimator from 1 μCi Sources in Acrylic Phantom

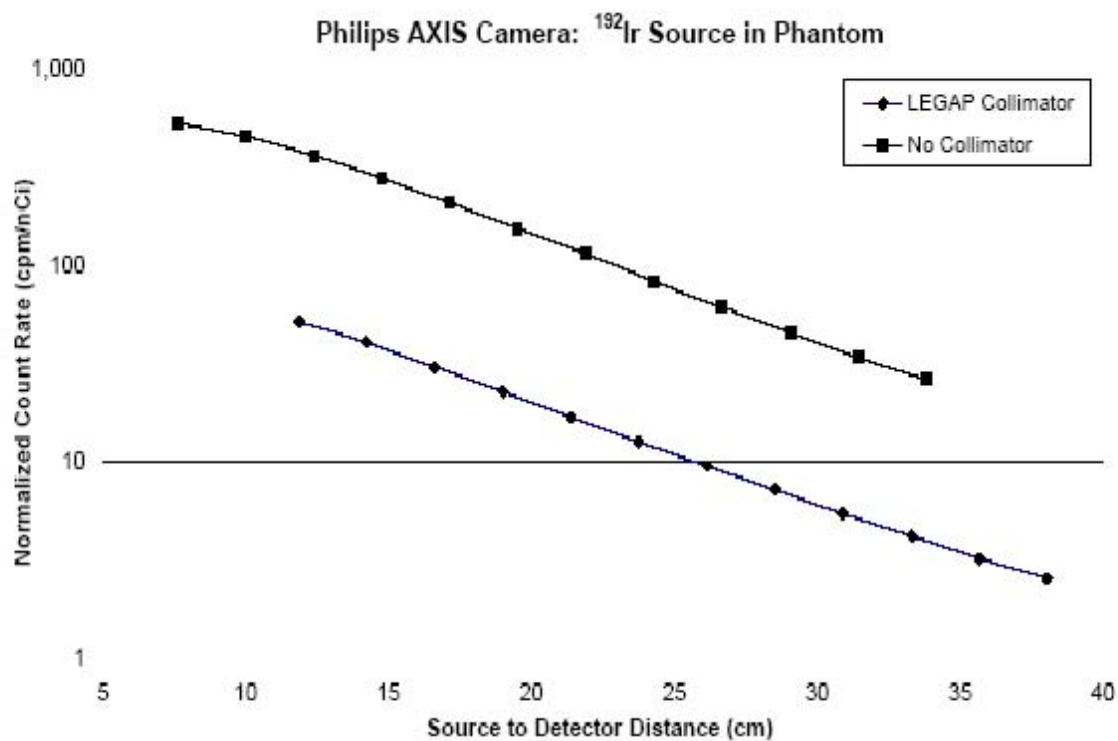


Figure 1-25. Normalized Count Rates in AXIS Camera from 18 μCi ^{192}Ir Source in Phantom

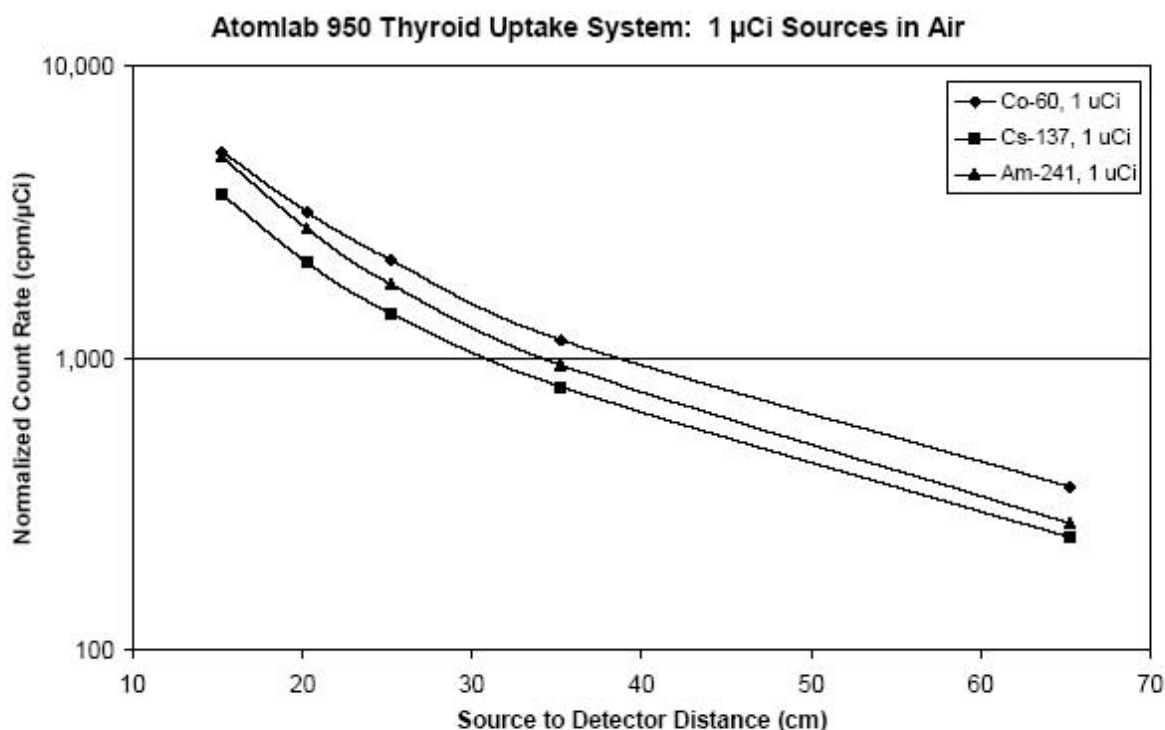


Figure 1-26. Normalized Count Rates in Atomlab 950 Thyroid Uptake System from 1 μ Ci Sources in Air

1.3.2 Thyroid Uptake System

Studies similar to those performed on the gamma cameras were carried out using the Atomlab 950 Thyroid Uptake System. The count rates from the nominal 1 μ Ci sources of ^{60}Co , ^{137}Cs , and ^{241}Am , as well as the nominal 10 μ Ci ^{241}Am source and the decayed ^{192}Ir therapy seed, were measured with the sources in air at varying distances from the face of the detector. The closest approach is 15.2 cm, the depth of the collimator (see description on page 1-11). Normalized count rates from the nominal 1 μ Ci sources as a function of distance from the detector are depicted in Figure 1-26,⁶ while the normalized counts from the ^{192}Ir source are shown in Figure 1-27.

As can be seen in these two figures, the normalized counts from ^{192}Ir are the highest of all the five sources tested with this instrument. This results from the fact that the γ -ray spectrum of ^{192}Ir primarily falls in the range of 300 – 600 keV. The 2×2 inch NaI crystal in this detector has

⁶ Normalized count rates from the nominal 10 μ Ci ^{241}Am source, which would almost exactly overlie the 1 μ Ci ^{241}Am data, are not shown on this graph.

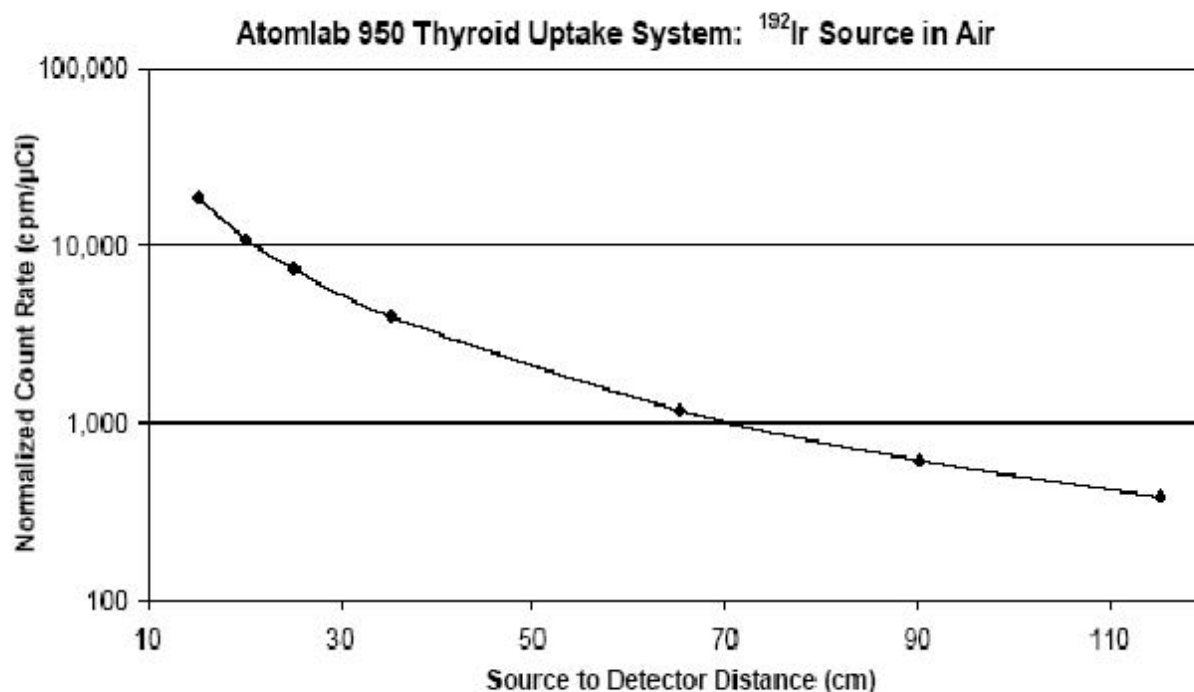


Figure 1-27. Normalized Count Rates in Atomlab 950 Thyroid Uptake System from 18 μCi ^{192}Ir Source

good sensitivity to photons in this energy range. Since this radionuclide emits about 210 photons in this energy range per 100 disintegrations, a high counting efficiency would be expected. While ^{60}Co emits 200 principal γ -ray photons per 100 disintegrations, these photons have energies of either 1173 or 1332 keV. Photons of these energies are less likely to interact with the NaI crystal—the detector is thus less efficient at counting photons of such high energies. ^{241}Am produces the third-highest counting rate. Although the 59.5 keV γ -ray photon emitted by this nuclide is efficiently captured by the NaI crystal, the lower intensity of this radiation—36 γ -ray photons are emitted per 100 disintegrations—leads to a lower normalized count rate. The lowest normalized count rate is from ^{137}Cs . This is due to the combination of the relatively high-energy γ ray (662 keV) which is not efficiently counted by the NaI crystal, and the fact that only 85.1 γ -ray photons are emitted per 100 disintegrations. Dead time counting losses do not appear to be significant for this instrument, judging from the fact that the 1 and 10 μCi ^{241}Am sources have virtually identical normalized rates.

Further studies were performed using the acrylic slab phantom. In these tests, the face of the phantom was put in contact with the edge of the collimator, placing it 15.2 cm from the face of the detector. One-microcurie sources of ^{60}Co , ^{137}Cs , and ^{241}Am were placed at various depths within the phantom. The normalized count rates from these three sources are displayed in [Figure 1-28](#). In this study, the ^{241}Am source produced the highest count rates at the surface of the phantom and at a depth of about 2.4 cm. At greater depths, the attenuation of the low-energy γ ray reduced the count rates below those of the other two nuclides. The greater attenuation of the ^{137}Cs γ rays with respect to those from ^{60}Co can be observed in the divergence of the two curves on the semilog plot.

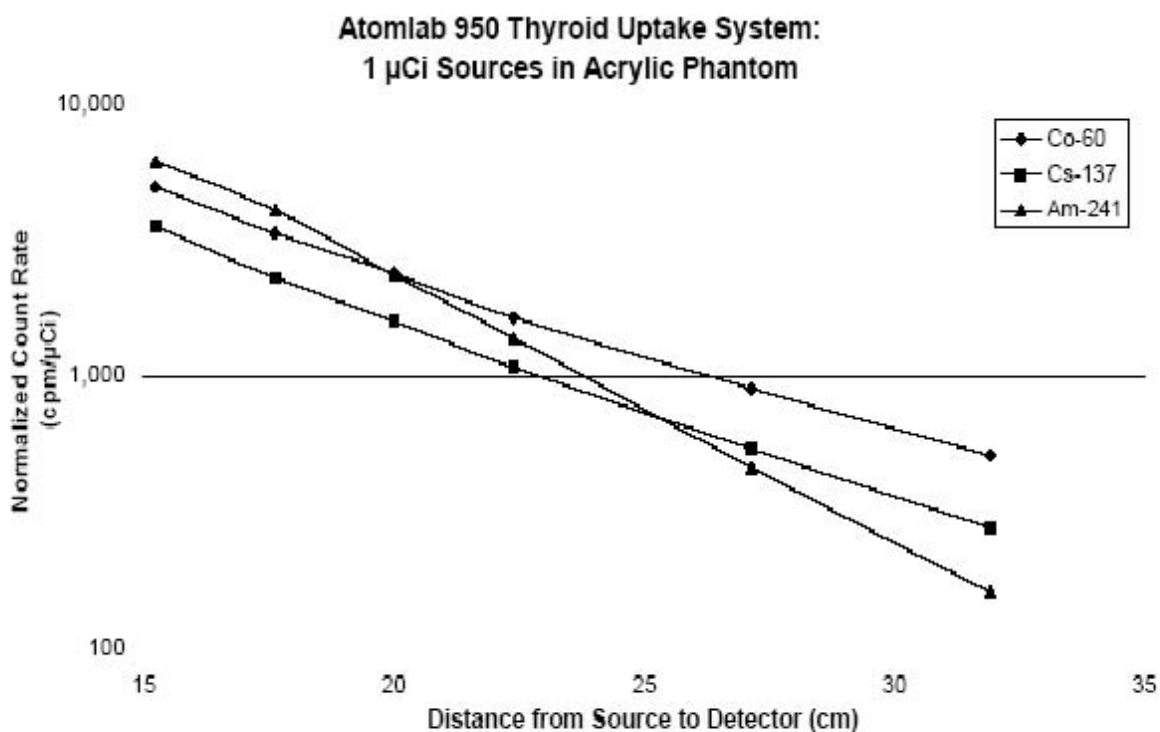


Figure 1-28. Normalized Count Rates in Atomlab 950 Thyroid Uptake System from 1 μ Ci Sources in Acrylic Phantom

1.3.3 Portal Monitor

As described on [page 1-12](#), the portal monitor system consists of two NaI detectors connected to a digital rate meter which is calibrated to display the count rate in terms of μ R/h. Thus, although the interactions of γ -ray photons with NaI detectors produce counts, not exposure, the count rate is translated into an exposure rate. The system is calibrated with a ^{137}Cs source—the scale on the rate meter is set to the calculated exposure rate at the location of the detector. According to information obtained from the manufacturer, 1 μ R/h corresponds to 1200 cpm when the radiation source is ^{137}Cs .⁷ For other photon energies, the reading is not a true exposure rate.

The exposure rates, as measured by the portal monitor, were recorded for the sealed sources used in the present study at various distances from the face of the single detector used in this experiment. [Figure 1-29](#) shows the normalized exposure rates from the seven sealed sources. The highest exposure rates are from ^{192}Ir , followed by ^{60}Co , as was the case for the thyroid uptake probe. However, the ^{137}Cs source produces a higher exposure rate than ^{241}Am . This reversal of the thyroid probe results most likely stems from the fact that the latter instrument uses pulse height analysis to isolate the photopeak of each radionuclide and thus does not count the low-energy scattered radiation from the high-energy γ emitters. Because the portal monitor

⁷ Bill Huckabee, Ludlum Measurements, Inc., private communication with Robert Anigstein, SC&A, Inc., March 14, 2005.

employs no energy discrimination, the scatter contributes to the total count rate. The normalized exposure rates from the higher-activity sources follow smooth curves out to the maximum distance of 105 cm from the detector. The actual recorded exposure rates from these higher-activity sources are well over 1 $\mu\text{R/h}$, and are thus readily distinguishable from background, which is typically about 1.5 $\mu\text{R/h}$ for this instrument in this location at HMC. For the 1 μCi sources, the normalized exposure rates are very close to the recorded exposure rates, since the actual activities of all three sources are within about 6% of their nominal values. Exposure rates much below 1 $\mu\text{R/h}$ exhibit irregular behavior, indicating that the readings are influenced by variations in background as well as by a lack of precision in the display of the rate meter, which reads in increments of 0.1 $\mu\text{R/h}$.

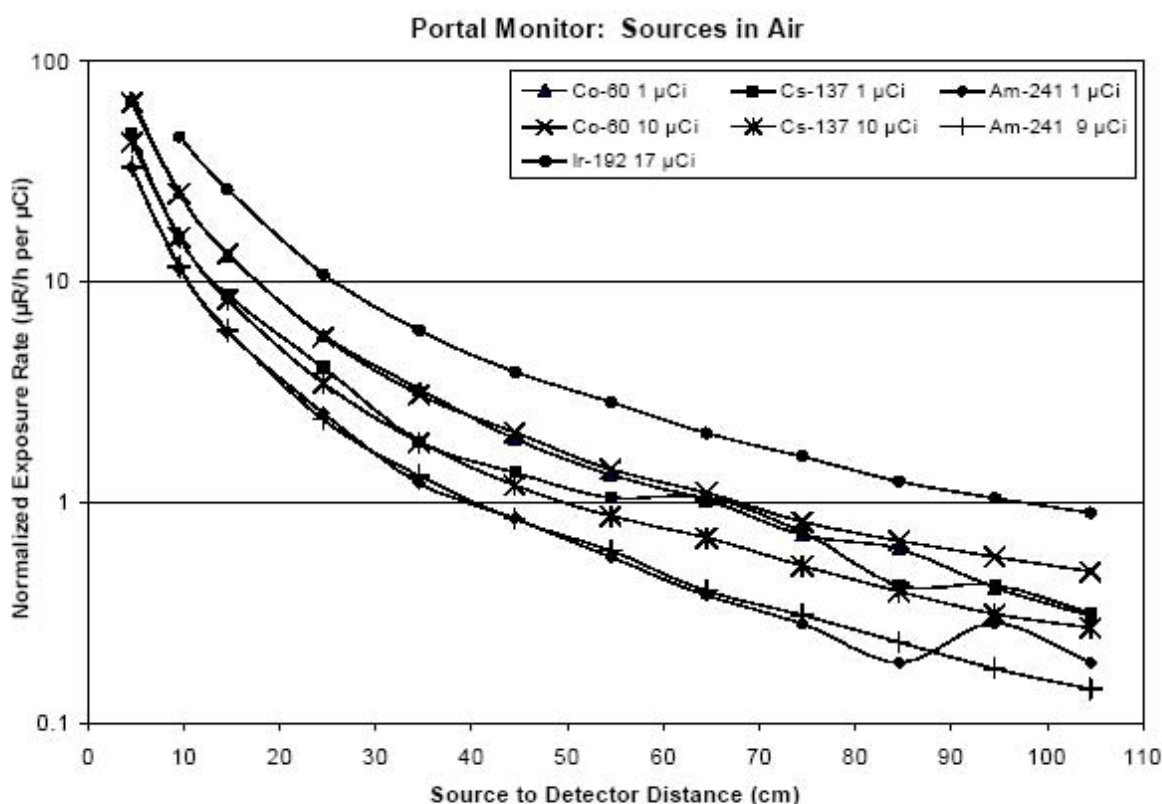


Figure 1-29. Normalized Exposure Rates Registered by Portal Monitor from Sources in Air

The effects of attenuation by the acrylic phantom on the portal monitor readings were tested by placing the source at a fixed distance from the detector and then inserting successive slabs of the acrylic phantom between the source and the detector. In this experiment, the three nominal 10 μCi sources and the ^{192}Ir seed were held at a distance of 29.3 cm from the detector and the exposure rate was recorded as up to 10 slabs of the acrylic phantom were placed between the source and the detector. The observed exposure rates were converted to normalized count rates, using the conversion factor: 1 $\mu\text{R/h} = 1200 \text{ cpm}$. As shown in Figure 1-30, all the nuclides except ^{241}Am show an increase in the count rate when one or two thicknesses of acrylic are placed between the source and the detector. This is probably due to the buildup of low-energy

photons in the plastic as a result of the Compton scattering of the relatively high-energy primary γ rays emitted by these nuclides. The 1-inch-thick NaI crystal has a higher absorption cross-section for these low-energy photons. The continuity of these curves indicates that all of these 9 to 17 μCi sources are detectable at depths of up to 24 cm in the acrylic phantom.

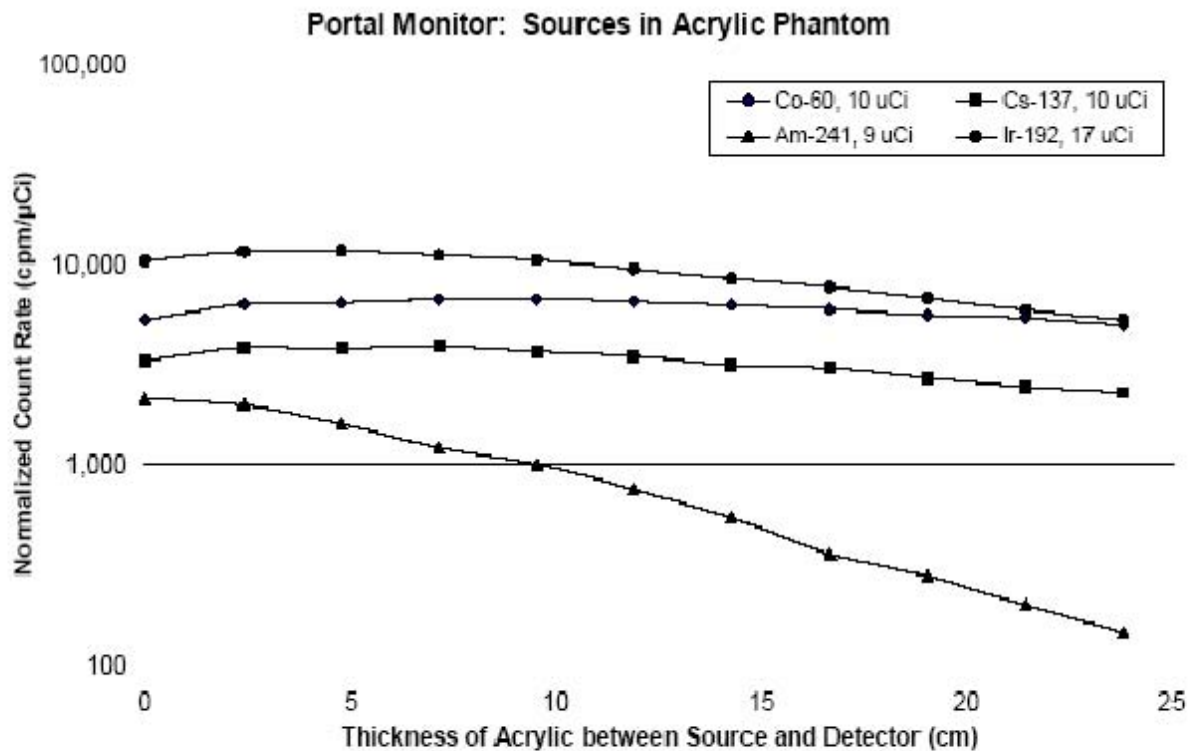


Figure 1-30. Normalized Count Rates, Converted from Portal Monitor Readings, from Sources in Acrylic Phantom

1.4 Detector Response to Discrete and Distributed ^{131}I Source in Water-Filled Phantom

All of the measurements discussed in the foregoing sections of the report involved discrete sources, either in air or at various depths within the acrylic slab phantom. In the case of an individual internally contaminated with radioactive materials, the activity would be dispersed in one or more organs. A series of experiments was performed to compare the response of the instruments to a discrete source in the center of a water-filled phantom to the same activity uniformly dispersed in the water. As stated earlier, ^{131}I was chosen for this study because it is readily obtainable in aqueous solution and is commonly used in nuclear medicine. Thus, the gamma cameras and the thyroid uptake system all have preset ^{131}I energy windows, which facilitates the measurements. The phantom used for this study is described and illustrated on page 1-3 of this report.

1.4.1 Gamma Cameras

One experiment involved the Philips SKYLIGHT camera equipped with the LEGP collimator and utilized the ^{131}I setting with a 20% energy window. The phantom with the discrete source (^{131}I in

an ampule) in the center, was placed at different distances from the face of the collimator, with the broad side of the phantom facing the camera. After the ampule was broken and activity dispersed in the water, the measurements were repeated, with the phantom in the same positions as before. The results, presented in Figure 1-31, show that the count rate from the distributed source, normalized to the total activity of the source at the time of the measurement, is consistently higher (by 15% to 22%) than from the discrete source for the same position of the phantom. These results are attributed to the fact that the half-value layer of water at 364 keV—the energy of the principal γ -ray of ^{131}I —is approximately 6 cm. Since the water jug is 16 cm thick, the source at the center is shielded by 8 cm of water, reducing the intensity of the γ ray by about 60%. Consequently, the activity near the front of the phantom makes a disproportionate contribution to the count rate.

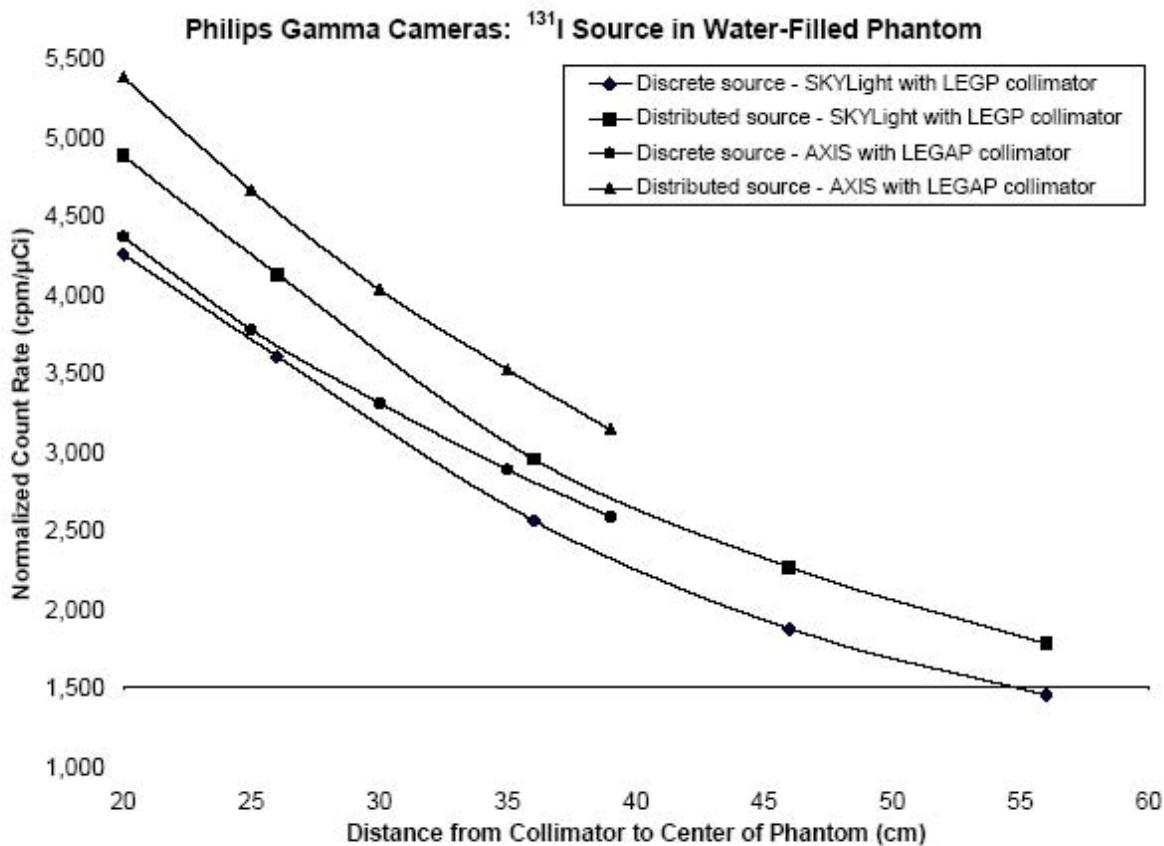


Figure 1-31. Count Rates in Philips Gamma Cameras from Discrete and Distributed ^{131}I Sources

The experiment was repeated using the Philips AXIS camera. The results, shown in Figure 1-31, indicate that the normalized count rate from the distributed source is consistently about 20% higher than the corresponding count rate from the discrete source. The count rates from the distributed source on the AXIS camera are somewhat higher than the comparable rates on the SKYLight. The count rates from the discrete source are also higher on the AXIS. This is

attributed to the greater counting efficiency of the AXIS unit, which has a thicker crystal ($\frac{3}{4}$ inch vs $\frac{3}{8}$ inch in the SKYLight) and a slightly larger field of view.

1.4.2 Thyroid Uptake System

Studies were performed of the response of the thyroid uptake system to discrete and distributed ^{131}I sources in the water-filled phantom. Two different orientations of the phantom were used in these studies. In both cases, the probe was pointed in a horizontal direction. In one case, the probe was centered on the broad side of the phantom—analogueous to an anteroposterior view of the body—while in the other case it was aligned with the center of the narrow side of the water jug—analogueous to a lateral view. In both cases, count rates, using the ^{131}I energy window built into the system, were measured with the phantom at varying distances from the detector.

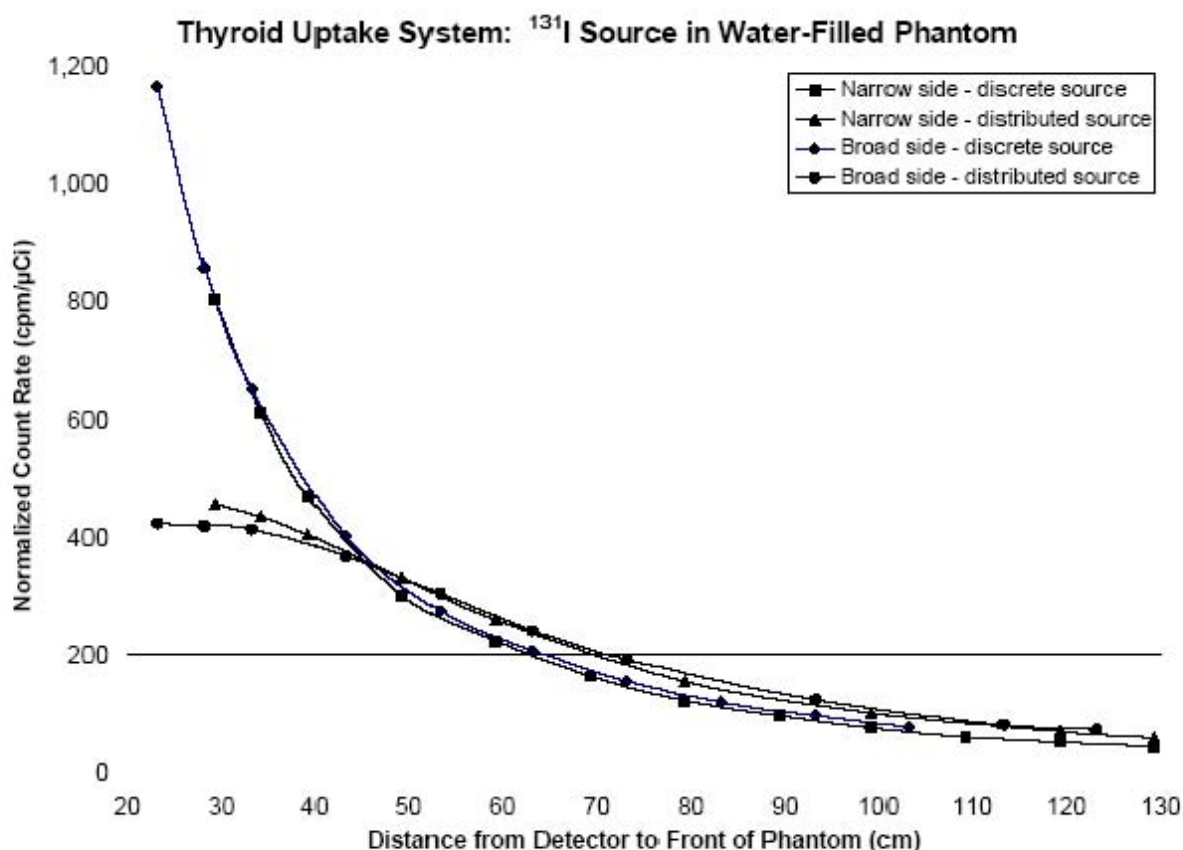


Figure 1-32. Count Rates in Atomlab 950 Thyroid Uptake System from Discrete and Distributed ^{131}I Sources

As shown in Figure 1-32, the count rates from the discrete source are significantly higher than from the distributed source when the phantom is nearest to the detector. As the distance increases, the two curves approach each other. In both orientations of the phantom, the curves cross when the center of the phantom is approximately 45 cm from the detector. This effect is

due to the narrow angle of view of the probe, as shown in the diagram in [Figure 1-15](#). Since the probe is designed to record activity in the thyroid gland, the collimator is designed to shield out radiation from elsewhere in the body. Thus, while the discrete source at the center of the water-filled jug is always within the field of view, the source that is distributed throughout the water-filled phantom is partially shielded by the collimator when the phantom is close to the detector. As the phantom is moved further away, more of the container comes into the field of view of the detector.

1.4.3 Portal monitor

The response of the portal monitor to discrete and distributed sources in the water-filled phantom was studied, using a protocol similar to that employed for the thyroid uptake system. One significant difference between the two systems that was cited earlier is the lack of pulse-height discrimination in the portal monitor. Thus, scattered radiation, which is mostly rejected by the thyroid uptake system, is counted by the portal monitor. The results, presented in [Figure 1-33](#), indicate little difference between the discrete source and the distributed source. Likewise, the count rates (recorded in units of $\mu\text{R/h}$), show little change with a 90° change in the orientation of the phantom.

1.5 Minimum Detectable Activity (MDA)

The minimum activity that can be detected by each of the instruments discussed in the foregoing sections depends on the background count rate of a given instrument in a given configuration, the counting time, and the observed count rate, normalized to the activity of the source. The following discussion is adopted from the MARSSIM manual (NRC 2000).

Two basic quantities related to the determination of the minimum detectable activity (MDA) are the critical level and the detection limit. Assuming that the background is counted for the same period of time as the suspected radioactive source, these quantities are defined as follows:

$$L_C = k \sqrt{2B}$$

$$L_D = k^2 + 2k \sqrt{2B}$$

L_C = critical level (counts)

L_D = detection level (counts)

k = Poisson probability sum for Type I and Type II errors

B = total background counts during counting period

A Type I error (“false positive”) occurs when a detector response is considered to be above background when, in fact, only background radiation is present. A Type II error (“false negative”) occurs when a detector response is considered background when, in fact,

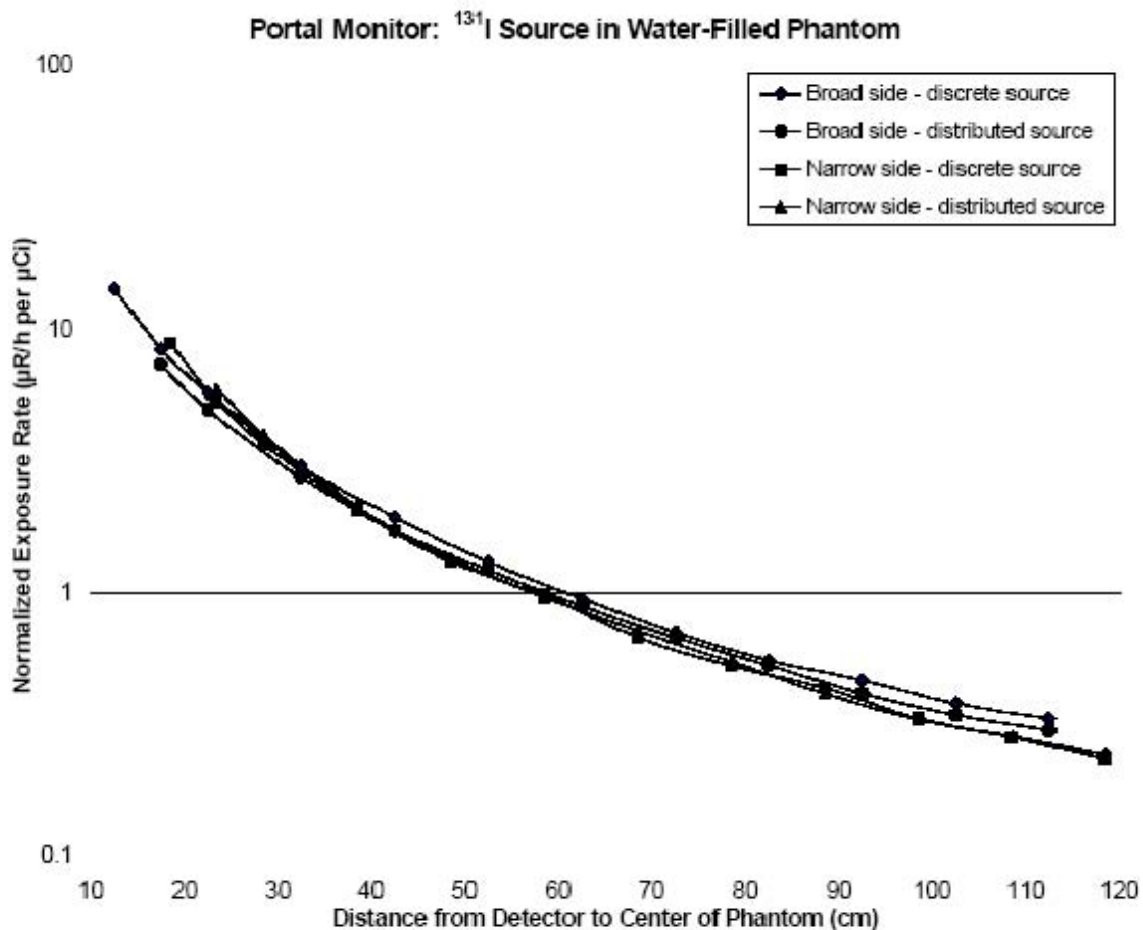


Figure 1-33. Exposure Rates on Portal Monitor from Discrete and Distributed ^{131}I Sources

radiation is present at levels above background. If values of .05 are considered acceptable for both Type I and Type II errors, then $k = 1.645$.

The previous equation is then written as

$$L_C = 2.33 \sqrt{B}$$

$$L_D = 3 + 4.65 \sqrt{B}$$

Note: NRC 2000 recommends evaluating k^2 as 3, based on Brodsky 1992.

Although any counts above the critical level are indicative of suspected radioactive contamination, only levels above the detection limit can be used to quantify the activity of any radioactive contaminants. In actual practice, the MDA is the product of the detection limit and

the normalized count rate of a given detector, in a given configuration, exposed to a given radionuclide:

$$A_{ijk} = \frac{3 + 4.65 \sqrt{\frac{b_{jk}}{t_c}}}{n_{ijk}}$$

A_{ijk} = minimum activity of radionuclide i detectable by detector j in configuration k

n_{ijk} = normalized count rate of detector j in configuration k exposed to radionuclide i

b_{jk} = background count rate of detector j in configuration k (cpm)

t_c = counting time for both background and patient (min)

Note: “configuration” refers to both the settings of the detector system (i.e., peak energy and width of energy window) and the source geometry (e.g., distance, thickness of phantom).

1.5.1 Phantom Studies

Minimum detectable activities (MDAs) were calculated for representative configurations of each detector system and each of the four principal radionuclides in the present study. The calculations are for a discrete source at selected depths within the acrylic phantom that correspond to activity distributed in the lungs. The appropriate locations within the acrylic phantom were selected by comparing this phantom to the phantoms (mathematical models of Reference Man) that are used to calculate radiation transport in the human body.

In the mathematical phantom of a 21-year-old male, based on the description by Cristy and Eckerman (1987), the chest wall has a thickness of 2.1 cm and an average density of 1.04 g/cm³, resulting in a mass thickness of 2.18 g/cm². This is comparable to one slab of the acrylic phantom, which has a nominal thickness of 2.38 cm and a density of 1.19 g/cm², resulting in a mass thickness of 2.83 g/cm². The maximum dimension in the anteroposterior direction (i.e., front to back) of the lung cavity in the Cristy phantom is 14.4 cm. The lung region of this model has a density of 0.296 g/cm³, yielding a mass thickness of 4.26 g/cm². Thus, the total mass thickness from the front of the chest to the rear of the lung cavity is 6.45 g/cm². This falls between the mass thickness of two slabs of acrylic—5.67 g/cm²—and that of three slabs—8.50 g/cm². Therefore, depths of 2.4, 4.8, and 7.1 cm, corresponding to one, two, and three slabs of the acrylic phantom, were selected to represent the response of detector systems to radionuclides in the lung.

The normalized count rates recorded by the AXIS camera, with and without a collimator, from sources at different depths in the acrylic phantom, are listed in [Table 1-4](#). In all cases, using the camera without a collimator would result in lower MDAs.

Table 1-4. Normalized Count Rates for AXIS Camera and MDAs Using Various Counting Times for Sources in Acrylic Phantom

	Nuclide	Background (cpm)	Depth (cm)	Count rate (cpm/nCi)	Counting time (min)				
					1	2	3	5	10
					MDA (nCi)				
No Collimator	Co-60 ^a	18,200	2.4	303.6	2.1	1.5	1.2	0.9	0.7
			4.8	253.0	2.5	1.8	1.4	1.1	0.8
			7.1	211.3	3.0	2.1	1.7	1.3	1.0
	Cs-137 ^b	2,200	2.4	108.7	2.0	1.4	1.2	0.9	0.7
			4.8	70.7	3.1	2.2	1.8	1.4	1.0
			7.1	47.6	4.6	3.3	2.7	2.1	1.5
	Ir-192 ^c	22,000	2.4	454.0	1.5	1.1	0.9	0.7	0.5
			4.8	361.2	1.9	1.4	1.1	0.9	0.6
			7.1	277.8	2.5	1.8	1.4	1.1	0.8
	Am-241 ^d	26,700	2.4	206.6	3.7	2.6	2.1	1.7	1.2
			4.8	131.4	5.8	4.1	3.4	2.6	1.9
			7.1	84.5	9.0	6.4	5.2	4.1	2.9
LEGAP Collimator	Co-60 ^a	9,300	2.4	129.7	3.5	2.5	2.0	1.6	1.1
			4.8	106.3	4.2	3.0	2.5	1.9	1.4
			7.1	85.9	5.3	3.7	3.0	2.4	1.7
	Cs-137 ^b	1,600	2.4	25.2	7.5	5.3	4.4	3.4	2.5
			4.8	17.9	10.6	7.5	6.2	4.8	3.5
			7.1	12.6	15.0	10.7	8.8	6.8	4.9
	Ir-192 ^c	9,522	2.4	40.6	11.3	8.0	6.5	5.1	3.6
			4.8	30.3	15.1	10.7	8.7	6.8	4.8
			7.1	22.6	20.2	14.3	11.7	9.1	6.5

^a 1 μ Ci source counted in 100% ¹³⁷Cs energy window

^b 1 μ Ci source counted in 20% ¹³⁷Cs energy window

^c 18 μ Ci source counted in 100% ¹⁸F energy window

^d 1 μ Ci source counted in 100% ¹³³Xe energy window

The normalized count rates recorded by the thyroid uptake system from sources at different depths in the acrylic phantom are listed in [Table 1-5](#). For all radionuclides except ²⁴¹Am, the MDAs are higher than those calculated for the AXIS camera, with or without a collimator. For ²⁴¹Am, the thyroid system has higher MDAs than the AXIS camera without a collimator. However, as noted earlier, microcurie sources of ²⁴¹Am could not be reliably counted on the AXIS system with the LEGAP collimator in place.

Table 1-5. MDAs for Atomlab 950 Thyroid Uptake System
Using Various Counting Times for Sources in Acrylic Phantom

Nuclide	Background (cpm)	Depth (cm)	Count rate (cpm/nCi)	Counting time (min)				
				1	2	3	5	10
				MDA (nCi)				
Co-60	56	2.4	3.31	11.4	8.3	7.0	5.6	4.2
		4.8	2.37	15.9	11.6	9.7	7.8	5.9
		7.1	1.63	23.1	16.9	14.1	11.4	8.6
Cs-137	62	2.4	2.28	17.4	12.7	10.6	8.5	6.4
		4.8	1.58	25.0	18.2	15.2	12.2	9.2
		7.1	1.07	37.0	27.0	22.6	18.1	13.6
Ir-192	186	2.4	12.27	5.4	3.9	3.2	2.6	1.9
		4.8	8.22	8.1	5.8	4.8	3.8	2.8
		7.1	5.62	11.8	8.5	7.1	5.6	4.1
Am-241	34	2.4	4.02	7.5	5.5	4.6	3.8	2.9
		4.8	2.33	12.9	9.5	8.0	6.5	5.0
		7.1	1.37	21.9	16.1	13.6	11.0	8.4

As is discussed on [page 1-25](#), the exposure rates recorded by the portal monitor were converted to count rates. Steinmeyer (1998) states that the effective counting time for a detector connected to a rate meter is twice the time constant of the rate meter. However, as stated on [page 1-14](#), the specifications for the rate meter on the Ludlum waste monitor cite the response time rather than the time constant. Steinmeyer addresses this issue by stating that according to a Ludlum report, the time constant is approximately equal to 44% of the response time. Thus, since the response time of the rate meter on the portal monitor is 3 seconds, the effective counting time is 2.64 s ($2 \times .44 \times 3 = 2.64$). The normalized count rates (converted from the exposure rates shown on the rate meter) and the calculated MDAs for the portal monitor system are shown in Table 1-6. As would be expected for an instrument that has a high background count rate relative to its counting efficiency and a short effective counting time, the MDAs are higher than for the gamma camera or the thyroid uptake system. Nevertheless, this instrument can play a useful role in screening individuals for internal radioactive contamination.

1.6 Calibration Factors

The normalized count rates listed in [Tables 1-4](#) and [1-5](#) for the gamma camera and the thyroid uptake system, and the exposure rates presented in [Table 1-6](#) for the portal monitor system, can serve as the bases for provisional calibration factors for these instruments when they are used to survey individuals who may have inhaled radioactive materials. The most useful values are those for sources attenuated by two slabs of the acrylic phantom—i.e., sources at a depth of 4.8 cm. This location most closely approximates a source near the center of the lung. Although, strictly speaking, the acrylic phantom is not tissue-equivalent in terms of its elemental composition, the attenuation of photons in the energy range of the γ rays from ^{60}Co , ^{137}Cs and ^{192}Ir is primarily due to Compton scattering and is thus not strongly affected by the exact composition

of the material. The derivation of the calibration factors for the three types of instruments included in the present study is discussed in the following sections of the present report. Recommended calibration factors for these instruments are summarized in [Table 1-7](#).

Table 1-6. MDAs for Portal Monitor System for Sources in Acrylic Phantom

Nuclide	Background ^a (cpm)	Depth (cm)	Exposure rate (μR/μCi)	Count rate ^a (cpm/nCi)	MDA (nCi)
Co-60	1,680	2.4	5.3	6.4	143
		4.8	5.4	6.5	140
		7.1	5.6	6.7	136
Cs-137		2.4	3.2	3.8	238
		4.8	3.2	3.8	240
		7.1	3.3	3.9	233
Ir-192		2.4	9.7	11.7	78
		4.8	9.8	11.8	77
		7.1	9.3	11.2	82
Am-241		2.4	1.6	2.0	461
		4.8	1.3	1.6	571
		7.1	1.0	1.2	752

Note: Effective counting time: 2.64 s

^a Calculated from observed exposure rate

Table 1-7. Recommended Calibration Factors

Nuclide	AXIS Camera		Thyroid Uptake System ^a (cpm/ μCi)	Portal Monitor ($\mu\text{R}/\text{h}$ per μCi)
	No collimator (cpm/nCi)	LEGAP collimator (cpm/nCi)		
Co-60	253	106	884	5.4
Cs-137	71	18	591	3.2
Ir-192	361	30	3,067	9.8
Am-241	131	—	870	1.3

^a Calibration factors were reduced by a factor of 2.68 to compensate for the exposure geometry (see discussion on page 1-36).

1.6.1 Gamma Camera

The gamma camera studies are reasonable approximations of the response of the camera to radioactive material distributed in the lung region. In the studies without the collimator, the source at a depth of 4.8 cm in the acrylic phantom was 12.4 cm from the front of the detector. This is a reasonable approximation of the position of the center of the chest cavity of an individual facing the camera. Since the detector is recessed about 2 cm within the housing of the instrument, and since the center of the chest is about 9.3 cm from the front of the body (see discussion of anthropomorphic phantom on [page 1-31](#)), the distance from the detector to the centroid of the activity would be approximately 11.3 cm. Thus, the count rate recorded in the

experiment is a reasonably conservative estimate of the count rate from a discrete source in the center of the lungs.

In the experiments using the collimator, the source at a depth of 4.8 cm in the phantom was 13.7 cm from the collimator. This is 2.4 cm further than the center of the lungs, if the exposed individual's chest was pressed against the collimator. Furthermore, the studies using the water-filled phantom show that the camera (with the collimator in place) is somewhat more sensitive to the source distributed throughout the volume of water than to a discrete source with the same total activity at the center of the phantom. Consequently, the count rate from the source in the phantom is a reasonably conservative estimate of the count rate from activity uniformly distributed in the lungs. (Since the study of the distributed source was not carried out for the camera without a collimator, this conclusion may not necessarily apply to that configuration.) Overall, calibration factors for the AXIS camera based on these count rates are expected to yield reasonable estimates of the total activity in the lungs of each of the four radionuclides studied. However, these calibration factors apply only under the following conditions:

- Philips AXIS camera equipped with $\frac{3}{4}$ -inch crystal
- Factors for camera using collimator apply to the LEGAP collimator only
- Factors apply only to the energy window used for each radionuclide in the present study
- Activity can be estimated within a factor of 2 of the actual value

These preliminary values may be revised as a result of the Monte Carlo simulations which will be presented in a later chapter of the present report.

1.6.2 Thyroid Uptake System

The count rates in the thyroid uptake system from a discrete source inside the acrylic phantom are not as readily translated into calibration factors as are the gamma camera data. As shown in [Figure 15](#), the detector has a narrow angle of view that would not encompass the entire chest unless the exposed individual was placed at some distance from the probe. This effect is demonstrated by the data on the water-filled phantom, which are presented on [page 1-28](#). Therefore, the count rates from a discrete source that is 4.8 cm from the edge of the conical collimator, the position of the source in the acrylic phantom, are an overestimate of the count rates from a source distributed in the lung.

To approximate the response of the detector to activity distributed throughout the lung, we must first correct for the distance of the centroid of the activity from the front of the detector. Since the collimator provides a 15.2-cm standoff, and since the center of the chest is assumed to be 9.3 cm from the front of the body, the total distance is 24.5 cm. However, the source in the acrylic phantom is only 20 cm from the detector. We can correct for this difference by comparing the count rates from sources in air 20.2 and 25.2 cm from the detector, the distances included in the data shown in [Figures 1-26](#) and [1-27](#) that are nearest to the desired distances. The average ratio of the count rates at these two distance from the four radionuclides is 1.50. Next, we estimate

the count rates from the discrete ^{131}I source in the water-filled phantom at a distance of 24.5 cm from the detector by interpolating between the count rates at adjacent distances, using the data collected with the broad side of the jug facing the detector which are displayed in [Figure 1-28](#). We then estimate the count rate at the same distance from the same source dispersed in the phantom. The ratio of these interpolated count rates is equal to 1.78. We then multiply this factor by 1.50, the correction factor for the distance, and obtain an overall correction factor of 2.68. If we divide the observed count rates from sources at a depth of 4.8 cm in the acrylic phantom by this factor, we obtain approximate calibration factors for the four radionuclides distributed in the lung. In actual practice, the count rates will be more variable than those obtained with the gamma camera. In the latter case, because of the large angle of view, the count rates are less sensitive to variations in the exact position of the exposed individual and to variations in body dimensions.

1.6.3 Portal Monitor

In the case of the portal monitor, the source was in the acrylic phantom was about 29 cm from the detector. The detector is shielded by a protective acrylic panel whose front surface is 4.5 cm from the face of the detector; therefore, in an individual whose chest is pressed against the acrylic panel, the center of the chest would be about 14 cm from the detector. Data from the study on the water-filled phantom indicates that the count rates from the discrete source are about 15% higher than from the same source dispersed in the phantom. Based on these observations, we can conclude that the calibration data for the portal monitor would enable reasonably conservative estimates of activity in the lungs of an exposed individual, the lowered count rate from the activity distributed in the chest being compensated by a closer distance to the detector. These results show that the portal monitor, if closely watched by a trained observer, is a useful screening tool for inhaled activities of any of the three β - γ emitters addressed in this study.

1.6.4 Application of Results

Of the three instruments on which definitive measurements were performed, the AXIS camera without a collimator is by far the preferred system for assessing individuals with radioactive material that is deposited in the lungs. However, the calibration factors for this instrument apply only to the four radionuclides addressed by the present study, only to the AXIS camera with a $\frac{3}{4}$ -inch crystal, and only to the energy window for each radionuclide listed in the footnotes to [Table 1-4](#). Data for different energy windows and for an AXIS camera with a $\frac{3}{8}$ -inch crystal, which is more representative of gamma cameras in nuclear medicine departments, are calculated using Monte Carlo simulations that will be presented in a later chapter of the present report.

1.7 Dose Calculations

The effective doses that could be received by an individual as a result of the failure of these instruments to detect activity deposited in the lung are calculated from the MDAs and the dose coefficients for the inhalation of the radionuclides in question. The dose coefficients are listed in ICRP Publication 68 (ICRP 1994) for different chemical forms and particle sizes. In the absence

of information on the chemical form and particle size of radionuclides that could be dispersed by a RDD, it is assumed that each radionuclide would have the chemical form and particle size that delivers the highest dose via the inhalation pathway. The calculations equate the activity present in the lungs at the time the individual is assessed to the activity inhaled by that individual.

The doses were calculated based on the MDAs of sources attenuated by two slabs of the acrylic phantom—i.e., those at a depth of 4.8 cm. As shown in Table 1-8, discrete sources of the three β - γ emitters— ^{60}Co , ^{137}Cs and ^{192}Ir —can be detected by any of the three radiation detection systems at levels that would correspond to doses of less than 15 mrem (150 μSv), which are much lower than the annual dose from natural background radiation and thus pose minimal risks to the exposed individual. This is not the case for ^{241}Am . The combination of the high-LET α radiation and the low-energy, low-intensity γ ray emitted by this radionuclide means that under the most favorable conditions—a 10-minute count by the gamma camera with no collimator—the MDA corresponds to a dose on the order of 300 mrem.

The same cautions cited in the discussion of the calibration factors apply to these MDA dose estimates. In addition, the MDAs and the corresponding doses are dependent on the background counting rates. The background rates may vary from one instrument to another. They are strongly affected by the presence of other radioactive sources in the vicinity as well as by natural background radiation. The MDAs for the thyroid uptake system listed in Table 1-8 were adjusted to reflect the adjustment to the calibration factors for this instrument discussed on page 1-36.

Table 1-8. Doses Associated with MDAs

Nuclide		Co-60		Cs-137		Ir-192		Am-241	
DCF (Sv/Bq)		2.90e-08		6.70e-09		6.20e-09		3.90e-05	
Detector	Time (min)	MDA (nCi)	Dose (mrem)	MDA (nCi)	Dose (mrem)	MDA (nCi)	Dose (mrem)	MDA (nCi)	Dose (mrem)
AXIS - no collimator	1	2.5	0.27	3.1	0.08	1.9	0.04	5.8	838
	3	1.4	0.15	1.8	0.05	1.1	0.03	3.4	485
	10	0.8	0.09	1.0	0.03	0.6	0.01	1.9	267
AXIS - with collimator	1	4.2	0.46	10.6	0.26	15.1	0.35	—	—
	3	2.5	0.26	6.2	0.15	8.7	0.20	—	—
	10	1.4	0.15	3.5	0.09	4.8	0.11	—	—
Thyroid uptake system ^a	1	42.7	4.59	67.0	1.66	21.7	0.50	34.6	4,993
	3	26.1	2.80	40.8	1.01	12.9	0.30	21.4	3,093
	10	15.8	1.70	24.7	0.61	7.5	0.17	13.3	1,919
Portal monitor		135.5	14.54	233.1	5.78	81.6	1.87	751.5	108,447

^a MDAs and calculated doses were increased by a factor of 2.68 to compensate for the exposure geometry (see discussion on page 1-36).

1.8 Conclusions

These preliminary studies of representative instruments found in nuclear medicine departments in hospitals and clinics show that such instruments can play a useful role in the screening and assessment of individuals who have inhaled airborne particles of radioactive materials. The three β - γ emitters— ^{60}Co , ^{137}Cs and ^{192}Ir —can be detected by any of these instruments at dose levels that are a small fraction of the annual doses from natural background radiation. The MDAs for ^{241}Am are much higher than for the other nuclides because the dose coefficient for the inhalation pathway is 3 or more orders of magnitude higher than for the other three nuclides. Thus, inhalation of ^{241}Am activities below the MDAs can produce doses ranging from over 250 mrem to over 100 rem, depending on the screening instrument and the counting time. Only a gamma camera with the collimator removed is appropriate for screening individuals potentially exposed to inhalation of this radionuclide.

References

- Amersham Health. 2004. *The Encyclopaedia of Medical Imaging*. Vol. 1. www.amershamhealth.com/medcyclopaedia/printout.asp?url=Volume%20I/ANGER%20CAMERA.html (March 29, 2005)
- Brodsky, A. 1992. "Exact Calculation of Probabilities of False Positives and False Negatives for Low Background Counting." *Health Physics*, 63(2), 198-204.
- Cristy, M., and K. F. Eckerman. 1987. "Specific Absorbed Fractions of Energy at Various Ages from Internal Photon Sources. I. Methods," ORNL/TM-8381/V1. Oak Ridge, TN: Oak Ridge National Laboratory.
- International Commission on Radiological Protection (ICRP). 1994. "Dose Coefficients for Intakes of Radionuclides by Workers," ICRP Publication 68. *Annals of the ICRP*, 24(4). Tarrytown, NY: Elsevier Science, Inc.
- Isotope Products Laboratories (IPL) 2003. "Reference & Calibration Sources." http://www.ipl.isotopeproducts.com/new_ipl_site/pdf/Std_Cat03.pdf (March 29, 2005).
- Marconi Medical Systems, Inc. 2001. "AXIS/IRIX Operator Guide," T55B-1465.D. Author.
- North American Scientific (NAS). 2005. "Gamma Source Calibration." <http://www.nomos.com/page?id=1481> (February 4, 2005).
- Nuclear Regulatory Commission (U.S.) (NRC). 2000. "Multi-Agency Radiation Survey and Site Investigation Manual (MARSSIM)," NUREG-1575, Rev. 1. Washington, DC: Author.
- Steinmeyer, P., Jr. 1998. "Detection Sensitivity and MDA (Part 1)." *Ludlum Report*, 13(1) 2-3. <http://www.ludlums.com/ReNwsLtr/NwsLtr-42re.pdf> (March 29, 2005).